Supplemental Figure 1

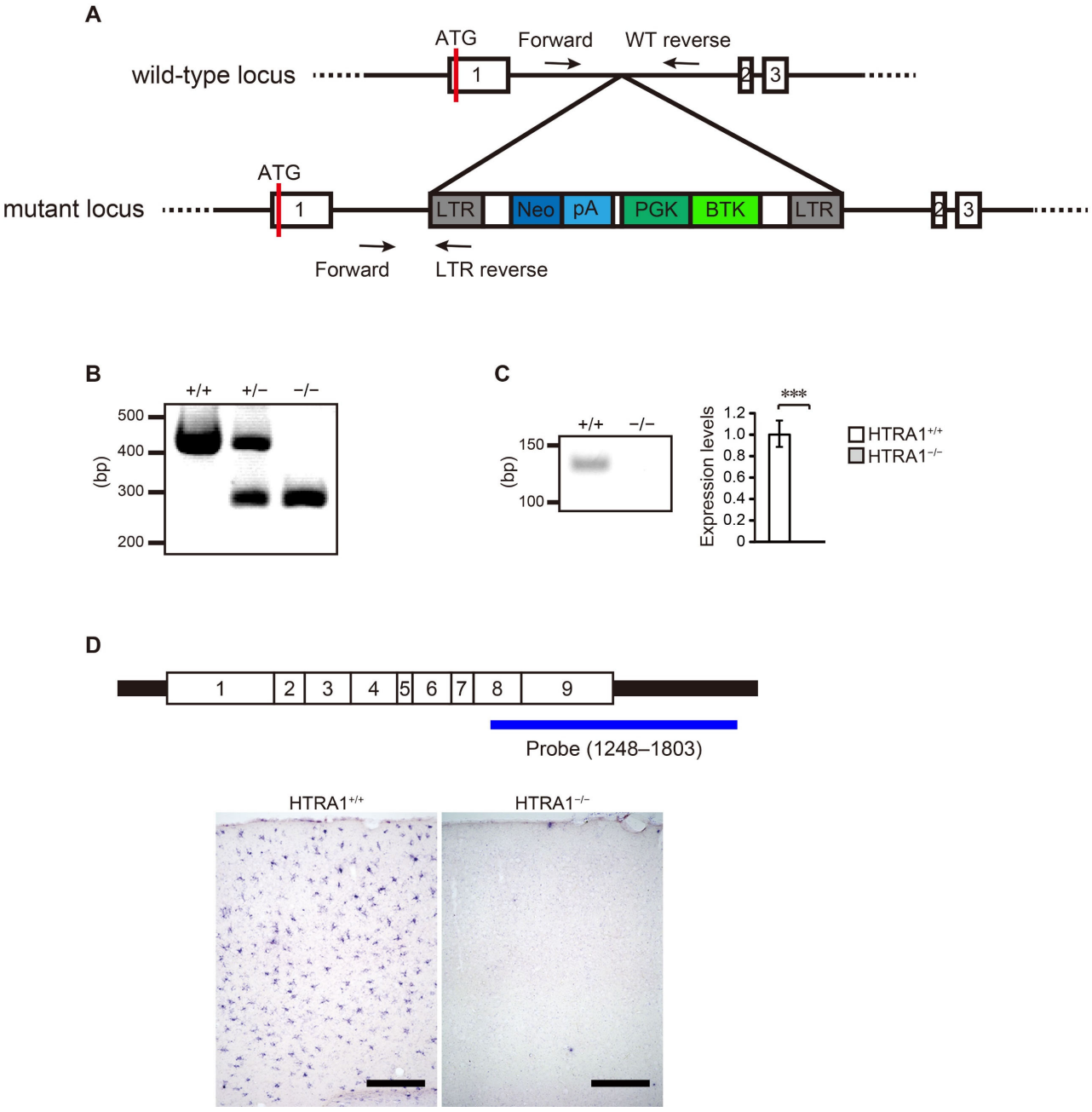

Supplemental Figure 1. Characterization of HTRA1$^{-/-}$ mice. (A) Genomic architecture of the *Htra1* gene in HTRA1$^{+/+}$ and HTRA1$^{-/-}$ mice. Omnibank gene trap vector 48 was inserted into the first intron of the *Htra1* gene between exon 1 and exon 2. The trap vector bears a long terminal repeat (LTR), a neomycin resistance gene (Neo), a polyadenylation signal (pA), a phosphoglycerate kinase 1 (PGK) promoter, and a Bruton tyrosine kinase (BTK) exon. The arrows depict positions of the primers using genotyping. **(B)** Mouse genotyping by PCR. A wild-type allele was detected using primers flanking the trap vector insertion site. The mutant allele was detected using a reverse primer located within the trap vector. **(C)** Deficiency in HTRA1 expression was validated by qRT-PCR analysis of total RNA extracted from the brain. The primers used for qRT-PCR targeted exon 5 and exon 6 of the mouse *Htra1* gene. The bar graph shows the relative levels of *Htra1* mRNA in the brains of 4-month-old HTRA1$^{+/+}$ mice, as determined by qRT-PCR analysis (n = 5–6 mice per group). The data represent the mean ± s.d. ***P < 0.001 with two-tailed unpaired t-test. **(D)** The upper diagram shows a schematic representation of *Htra1* mRNA and the location of the probe used for in situ hybridization (depicted by the blue line). The lower images of the cerebral cortex show specificity of the antisense probe as confirmed using HTRA1$^{+/+}$ and HTRA1$^{-/-}$ mouse tissues. *Htra1* mRNA expression was detected in HTRA1$^{+/+}$ mouse tissue only, demonstrating the specificity of our antisense probe, which was used in the following analysis. Scale bar = 100 μm.

Supplemental Figure 2

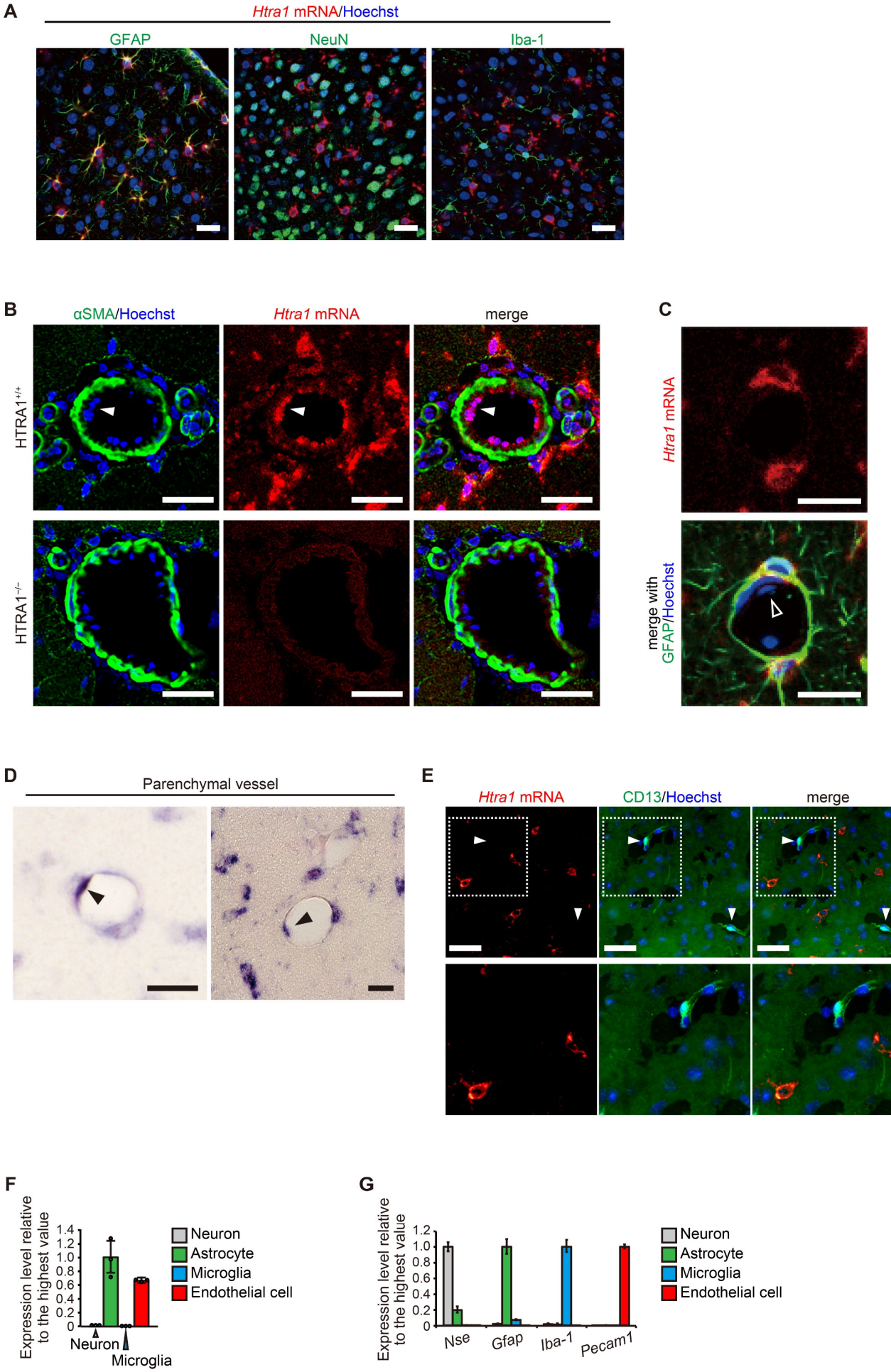

Supplemental Figure 2. Cellular distribution of *Htra1* mRNA in the mouse brain. (A) Simultaneous detection of *Htra1* mRNA and GFAP, NeuN, or Iba-1 in the brains of HTRA1$^{+/+}$ mice. The combination of in situ hybridization and immunostaining revealed colocalization of GFAP immunoreactivity with the signals for *Htra1* mRNA in the brain. Scale bar = 20 μm. **(B)** Simultaneous detection of *Htra1* mRNA and αSMA in pial arteries (longitudinal cerebral fissure). In the pial arteries of HTRA1$^{+/+}$ mice, endothelial cells were positive for *Htra1* mRNA (filled white arrowhead). These *Htra1* mRNA signals in endothelial cells were absent in HTRA1$^{-/-}$ mice. Scale bar = 25 μm. **(C)** Simultaneous detection of *Htra1* mRNA and GFAP in the brains of HTRA1$^{+/+}$ mice. Perivascular astrocytes surrounding parenchymal small vessels expressed *Htra1* mRNA. In contrast to those of pial arteries, most endothelial cells of parenchymal small vessels lacked an *Htra1* mRNA signal (empty arrowhead). Scale bar = 10 μm. **(D)** The images show *Htra1* mRNA signals in the intracerebral vasculature, which was rarely detected by NBT/BCIP chromogenic stain (arrowhead). We found that most endothelial cells on brain arterioles (precapillaries) or capillaries were negative for *Htra1* mRNA even when detected by NBT/BCIP detection (1). Scale bar = 10 μm. **(E)** Simultaneous detection of *Htra1* mRNA and the pericyte marker CD13. The lower image is a high-magnification image of the upper micrograph. Arrowheads indicate the location of pericytes in each image. Scale bar = 50 μm. **(F and G)** Quantification of *Htra1* mRNA expression levels in primary culture neurons, astrocytes, microglia, and endothelial cells by qRT-PCR analysis (n = 3 per group) **(F)**. HTRA1$^{+/+}$ mouse brains were used to establish primary cultures of each cell type. Each expression level was normalized by the expression levels of the reference gene set. The bar graph shows the expression level relative to astrocytes. **(G)** The mRNA levels of *Nse*, *Gfap*, *Iba-1*, and *Pecam1* in each primary culture were quantified to confirm the establishment of primary cultures of each cell type. Expression levels are presented as values relative to the highest expression level of each cell marker. The data represent the mean ± s.d.

Supplemental Figure 3

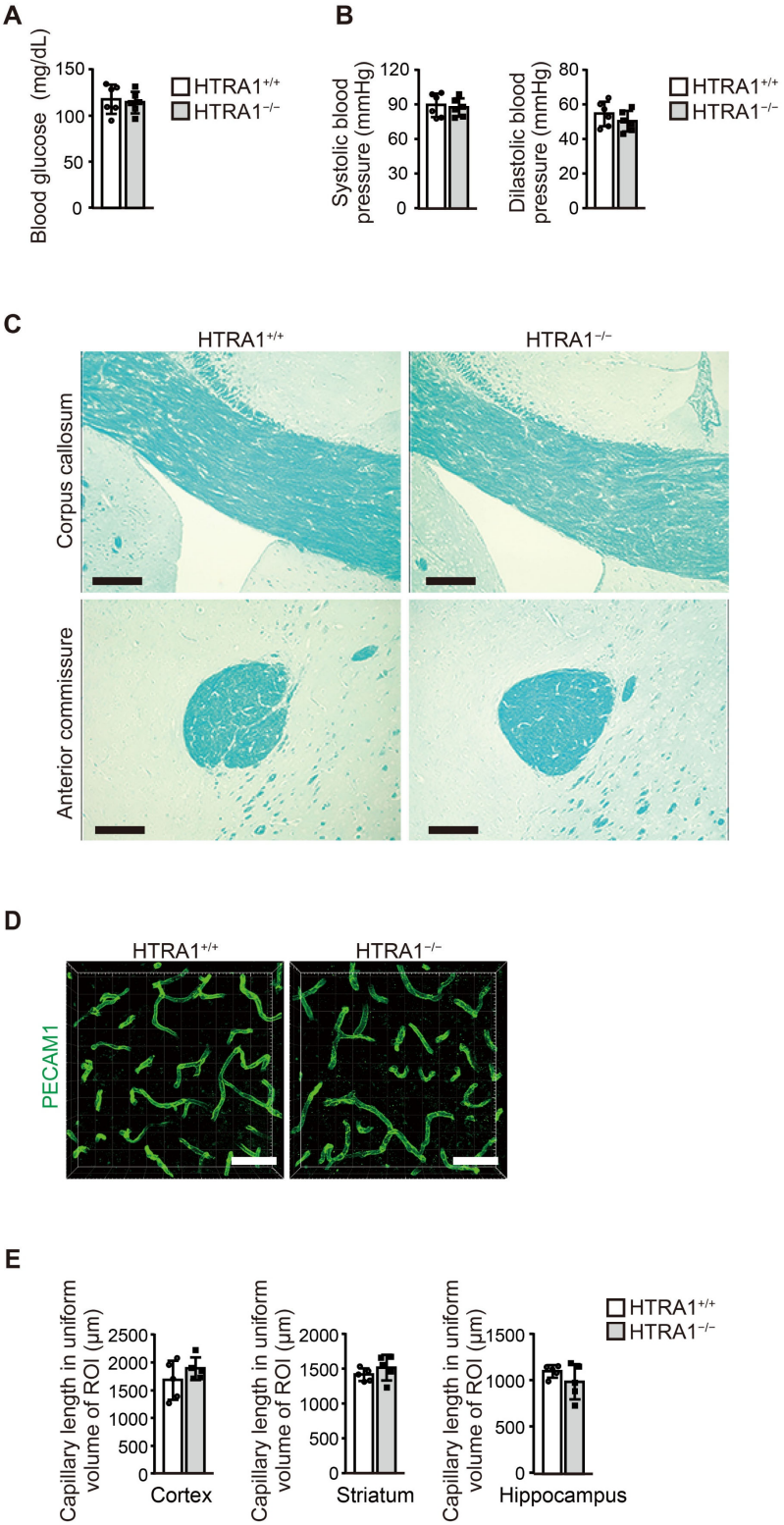

Supplemental Figure 3. Absence of gross neuropathological abnormalities in the white matter and brain capillaries. (A and B) Mouse blood glucose levels and blood pressure were evaluated at 16 months of age. HTRA1$^{-/-}$ mice had normal blood glucose **(A)** and blood pressure **(B)** levels that were indistinguishable from those of HTRA1$^{+/+}$ mice (n = 6 animals). **(C)** The brain white matter of HTRA1$^{+/+}$ and HTRA1$^{-/-}$ mice was examined at 24 months of age by Luxol fast blue staining. Typical images of the corpus callosum and the anterior commissure +0.86 mm from bregma are shown. There was no neuropathological sign of white matter lesions in any section prepared from three animals from each group. Scale bar = 50 μm. **(D and E)** Brain capillaries were visualized by immunostaining for PECAM1. The panels are representative images of PECAM1-immunopositive capillaries in the cerebral cortex **(D)**. Capillary length in a uniform volume of the brain was sterically measured using three-dimensional reconstructed images of the cerebral cortex, the striatum, and the hippocampus of 24-month-old HTRA1$^{+/+}$ and HTRA1$^{-/-}$ mice using the Imaris Filament Tracer **(E)**. The data represent the mean ± s.d. (n = 5 animals per group; 2 images per animal).

Supplemental Figure 4

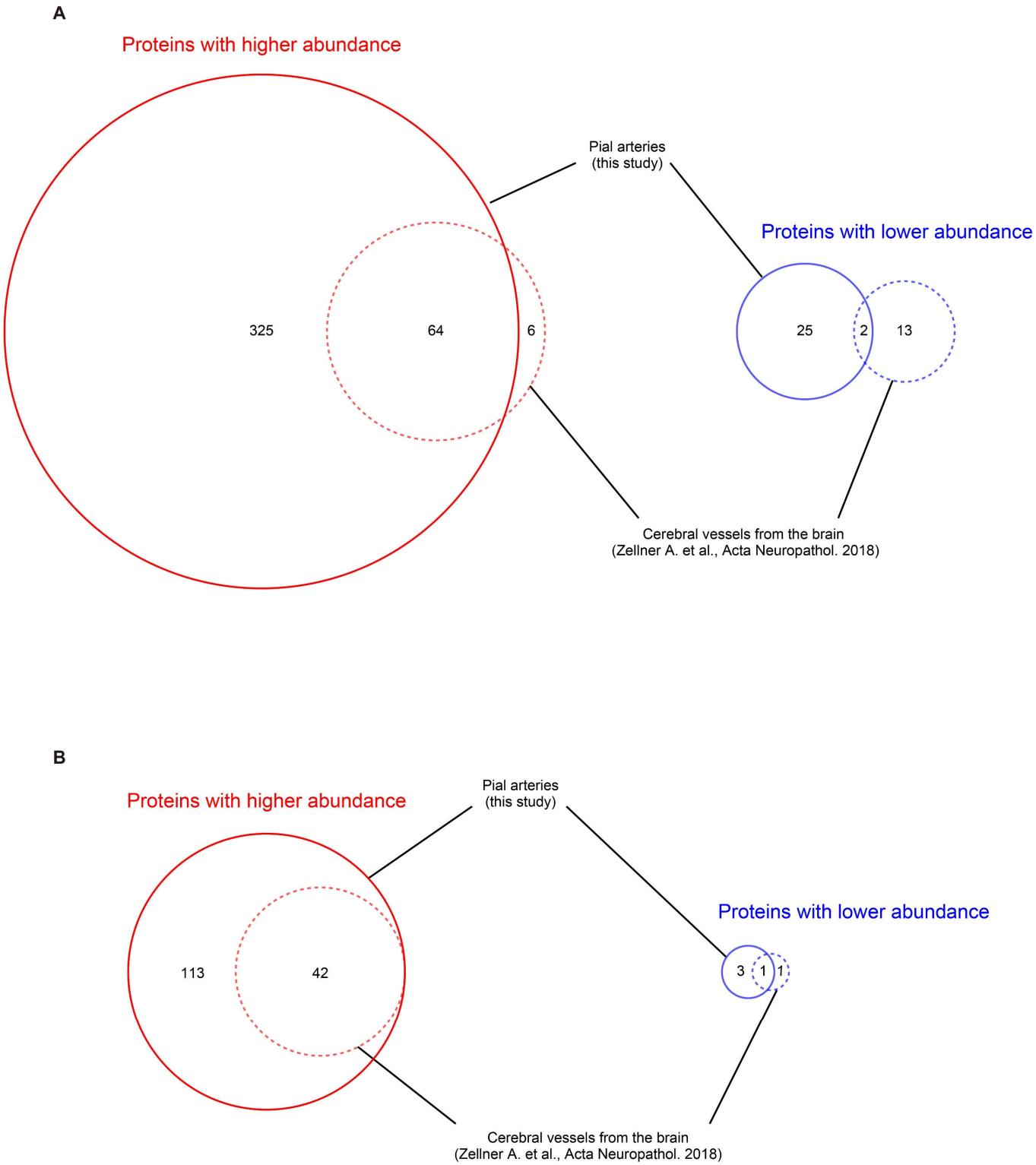

Supplemental Figure 4. Comparison of proteins that were altered in HTRA1$^{-/-}$ mice between independent study data sets. (A) Venn diagram showing the overlap of the two datasets consisting of all the proteins that were changed in HTRA1$^{-/-}$ mice. The red circles represent proteins that were significantly increased in HTRA1$^{-/-}$ mouse samples with a fold change in protein abundance > 1.5. The blue circles represent proteins that were significantly decreased in HTRA1$^{-/-}$ mouse samples with a fold change in protein abundance < 1.5^{-1}. **(B)** Venn diagram illustrating overlapping matrisome proteins according to categories defined by Naba et al. (2, 3) . The solid line circles indicate the datasets obtained in this study, and the dashed lines show the datasets obtained by Zellner et al. (4).

Supplemental Figure 5

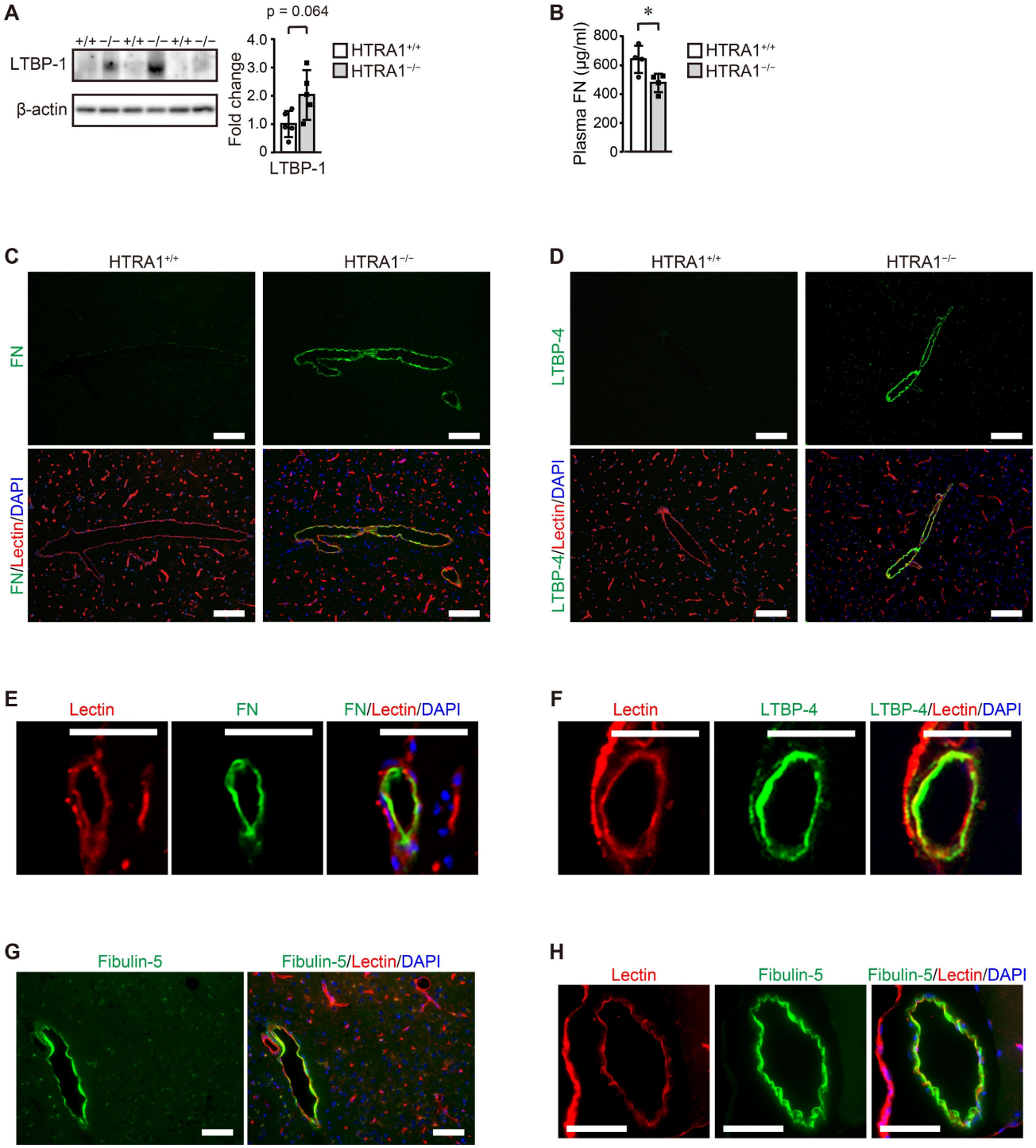

Supplemental Figure 5. Quantification of matrisome proteins in mouse cerebral arteries and blood samples and accumulation of matrisome proteins at pial arteries and arterioles but not capillaries. (A) Quantification of LTBP-1 in the anterior and middle cerebral arteries of 24-month-old HTRA1$^{+/+}$ and HTRA1$^{-/-}$ mice by immunoblotting analysis. The bar graphs show the value relative to that of HTRA1$^{+/+}$ mice (n = 5 animals per group). **(B)** Plasma FN content in 24-month-old HTRA1$^{+/+}$ and HTRA1$^{-/-}$ mice was quantified by ELISA. *P < 0.05 with two-tailed unpaired t-test (n = 4 animals per group). The data represent the mean ± s.d. **(C and D)** Accumulation of FN and LTBP-4 in the intraparenchymal arterioles of HTRA1$^{-/-}$ mice. Immunohistochemical analysis revealed that FN **(C)** and LTBP-4 **(D)** were deposited at arterioles but not capillaries (diameter < 5 μm) in the brains of HTRA1$^{-/-}$ mice. Vascular endothelial cells were visualized by DyLight 594-labeled tomato lectin (n = 3 animals per group). Scale bar = 100 μm. **(E and F)** Accumulation of FN and LTBP-4 in brain superficial small pial arteries. FN **(E)** and LTBP-4 **(F)** were deposited in small pial arteries of HTRA1$^{-/-}$ mice. Scale bar = 50 μm. **(G and H)** Accumulation of fibulin-5 in the intraparenchymal arterioles **(G)** and in brain superficial small pial arteries **(H)** of HTRA1$^{-/-}$ mice (n = 3 animals per group). Scale bar = 50 μm.

Supplemental Figure 6

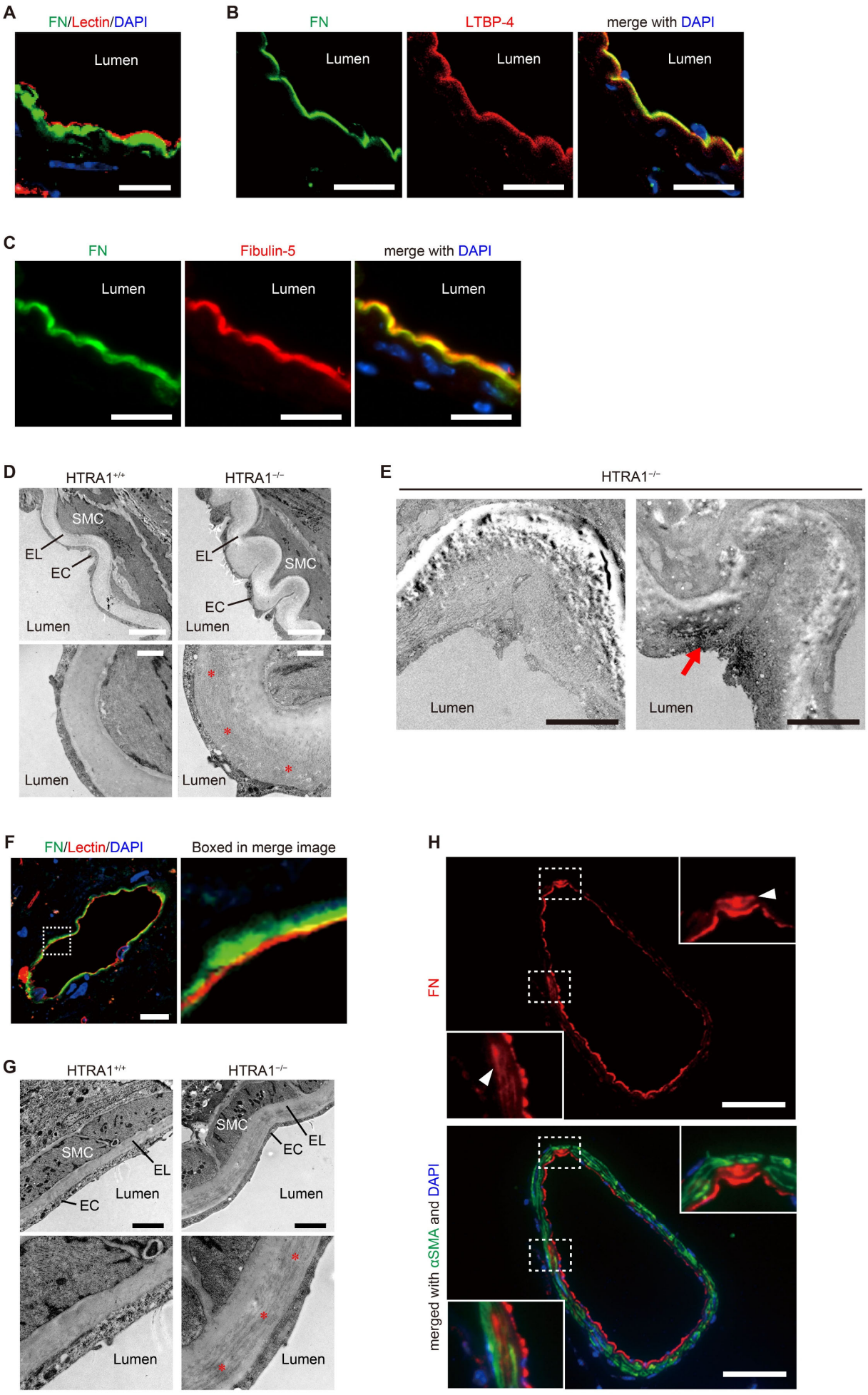

Supplemental Figure 6. Accumulation of FN, LTBP-4, and fibulin-5 within the arterial subendothelial space in HTRA1$^{-/-}$ mice. (A) The brains of twenty-four-month-old HTRA1$^{-/-}$ mice were subjected to immunohistochemical detection of FN with fluorescent lectin staining. FN accumulation was found in the subendothelial cell layer of the pial arteries in HTRA1$^{-/-}$ mice. Scale bar = 10 μm. **(B and C)** The brains of twenty-four-month-old HTRA1$^{-/-}$ mice were subjected to immunohistostaining for FN and LTBP-4 **(B)** or fibulin-5 **(C)** using Zenon labeling technology. FN and LTBP-4 or fibulin-5 were colocalized in the subendothelial cell layer of the pial arteries. Scale bar = 20 μm. **(D)** Upper: Electron micrographs of the pial arteries of HTRA1$^{+/+}$ and HTRA1$^{-/-}$ mice at 24 months of age showing intimal hyperplasia over the entire circumference of the arteries of HTRA1$^{-/-}$ mice (EC: endothelial cell; SMC: smooth muscle cell; EL: elastic lamina). Scale bar = 5 μm. Lower: High-magnification images of the intima of a pial artery revealed that a high-electron-dense layer (red asterisks) was formed in the subendothelial layer. Scale bar = 1 μm. **(E)** Validation of FN deposition in the thickened intima by immunoelectron microscopic analysis. Right: Electron microscopy analysis of pre-embedding 3,3′-diaminobenzidine immunostaining highlighting FN deposition (red arrow). Left: As a color reference control, slices from the same specimen were stained with eosin and then embedded for electron microscopy analysis. Scale bar = 2 μm. **(F)** Subendothelial accumulation of FN in the intraparenchymal arterioles of HTRA1$^{-/-}$ mice. Scale bar = 15 μm. **(G)** Upper: Electron micrographs of the intraparenchymal arterioles of HTRA1$^{+/+}$ and HTRA1$^{-/-}$ mice at 24 months of age showing intimal hyperplasia of the arteries of HTRA1$^{-/-}$ mice. Scale bar = 5 μm. Lower: High-magnification images of the intima revealed that a high-electron-dense layer (red asterisks) formed in the subendothelial layer. **(H)** Accumulation of FN in the tunica media (filled white arrowhead) in HTRA1$^{-/-}$ mice. Brain sections prepared from 24-month-old HTRA1$^{-/-}$ mice were immunostained with FN and αSMA. The insets are high magnifications of the boxed regions in each image. Scale bar = 50 μm.

Supplemental Figure 7

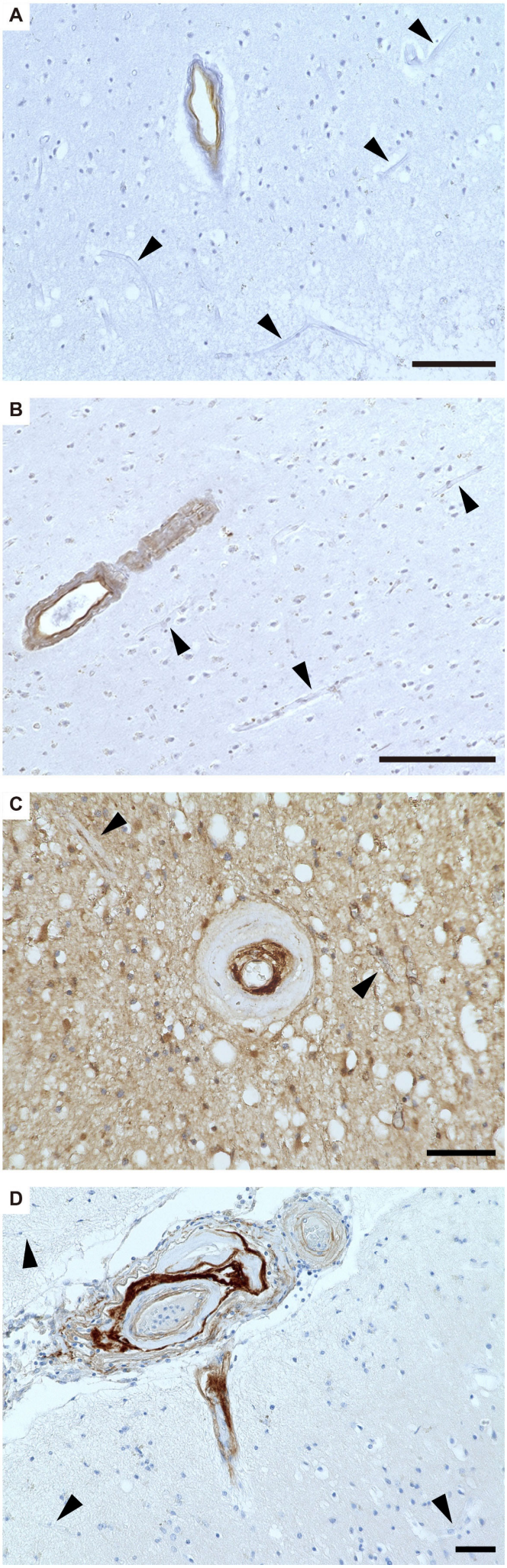

Supplemental Figure 7. Accumulation of matrisome proteins in the arterioles of CARASIL patients. (A–D) FN **(A)**, LTBP-4 **(B),** TIMP3 **(C),** and fibulin-5 **(D)** immunoreactivity in the parenchymal cerebral vessels of CARASIL patients. As in HTRA1$^{-/-}$ mice, matrisome proteins were deposited at the arterioles but not the brain capillaries (arrowheads). Scale bar = 50 μm.

Supplemental Figure 8

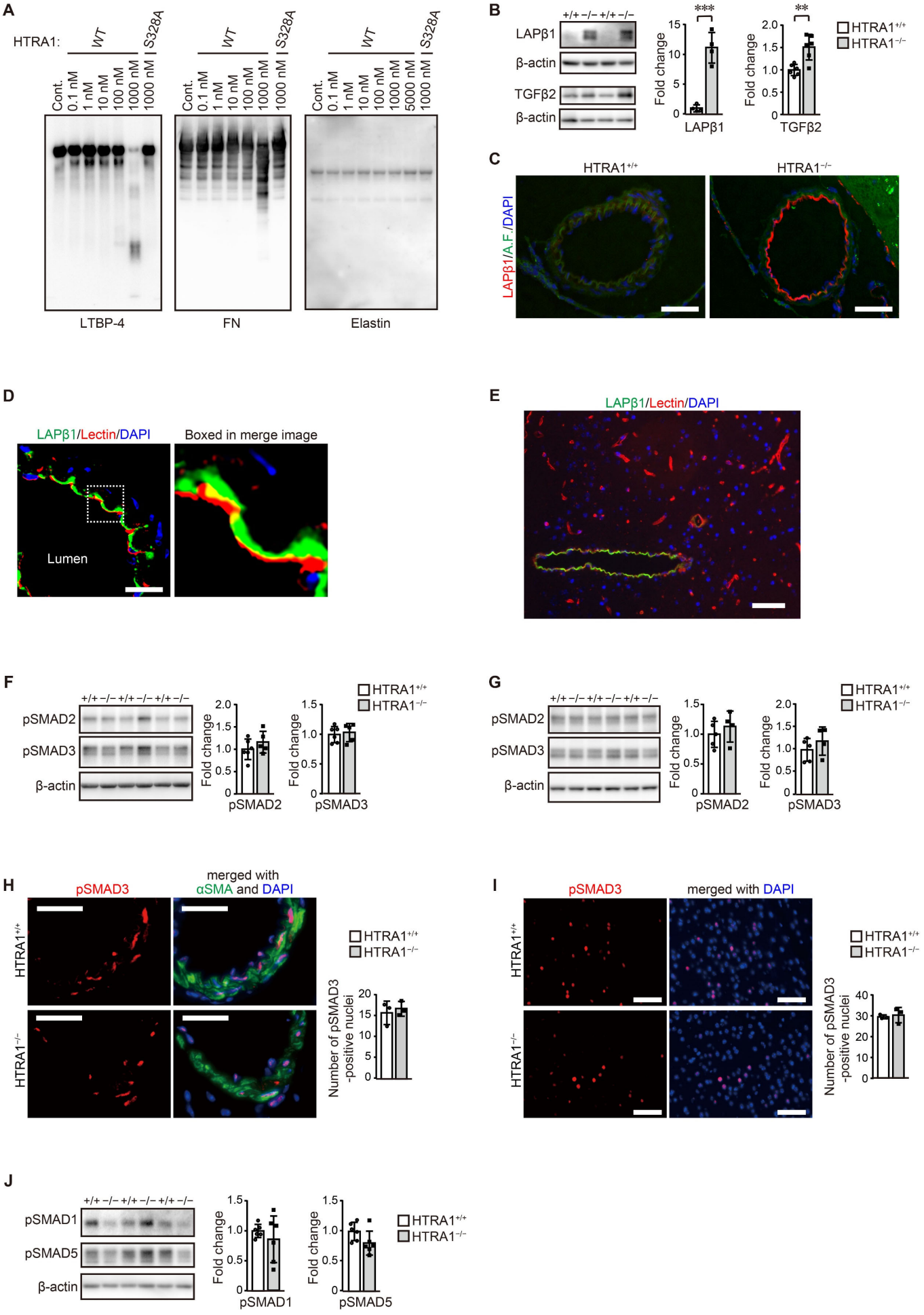

Supplemental Figure 8. In vitro digestion assay using HTRA1 and quantification of phosphorylated SMAD levels. (A) Human LTBP-4, FN, and elastin were treated with full-length recombinant human HTRA1 protein at the indicated concentrations for 6 h and then subjected to immunoblotting analysis. The HTRA1 protein with an amino acid substitution in the serine protease motif (S328A), which abolishes protease activity, was used as a negative control. **(B)** Protein levels of LAPβ1 and TGFβ2 in mouse anterior and middle cerebral arteries were assessed by immunoblotting at 24 months of age (n = 4–6 animals per group). **P < 0.01 and ***P < 0.001 with two-tailed unpaired t-test or the Mann-Whitney U-test. The samples used for LAPβ1 were distinct from those used for TGFβ2 quantification. **(C)** LAPβ1 in the anterior cerebral arteries was detected by immunohistostaining at 24 months of age. Scale bar = 50 μm. **(D and E)** The brains of twenty-four-month-old HTRA1$^{-/-}$ mice were subjected to immunohistochemical detection of LAPβ1 with fluorescent lectin staining. **(D)** LAPβ1 accumulation was found in the subendothelial cell layer of pial arteries in HTRA1$^{-/-}$ mice. Scale bar = 15 μm. **(E)** LAPβ1 deposition was observed in intraparenchymal arterioles but not capillaries. Scale bar = 30 μm. **(F and G)** Levels of pSMAD in the cerebral arteries **(F)** and cerebral cortices **(G)** were assessed by immunoblotting at 24 months of age (n = 4–6 animals per group). **(H and I)** The number of pSMAD3-immunopositive cell nuclei in the anterior cerebral arteries **(H)** and cerebral cortices **(I)** of HTRA1$^{+/+}$ and HTRA1$^{-/-}$ mice at 24 months of age. Vascular SMCs were visualized by αSMA immunostaining. Scale bar = 25 μm. (n = 3 animals per group; 5 images per animal). **(J)** The levels of pSMAD1/5 in the anterior and middle cerebral arteries were assessed by immunoblotting at 24 months of age (n = 6 animals per group). The data represent the mean ± s.d.

Supplemental Figure 9

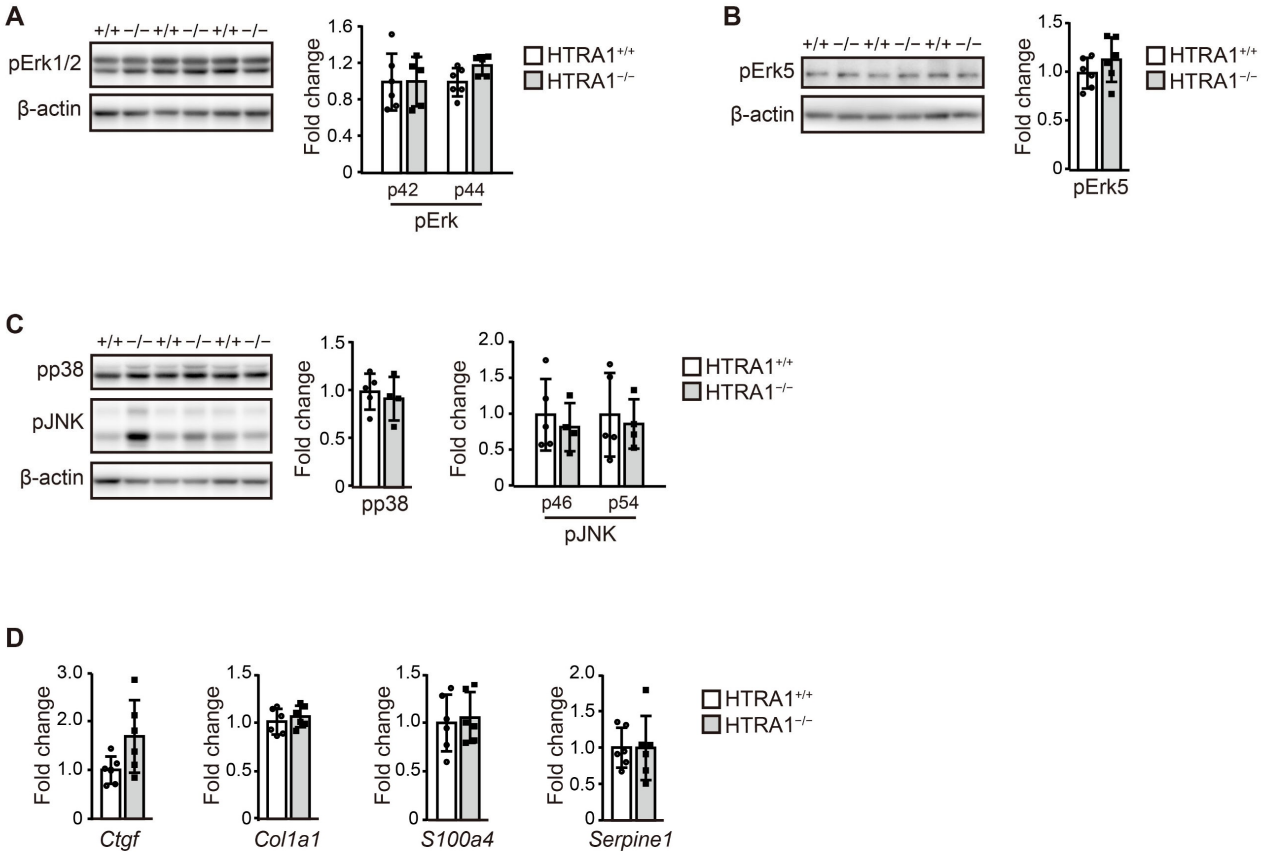

Supplemental Figure 9. SMAD-independent noncanonical pathway and quantification of the expression levels of genes regulated by TGFβ. (A–C) The levels of phosphorylated Erk1/2 (pErk1/2) **(A)**, pErk5 **(B)**, pp38, and pJNK **(C)** in the anterior and middle cerebral arteries were assessed by immunoblotting at 24 months of age (n = 4–6 animals per group). **(D)** The expression of genes regulated by TGFβ in the mouse anterior and middle cerebral arteries was quantified at 24 months of age (n = 6 animals per group). The bar graphs show the value relative to that of $HTRA1^{+/+}$ mice. The data represent the mean ± s.d.

Supplemental Figure 10

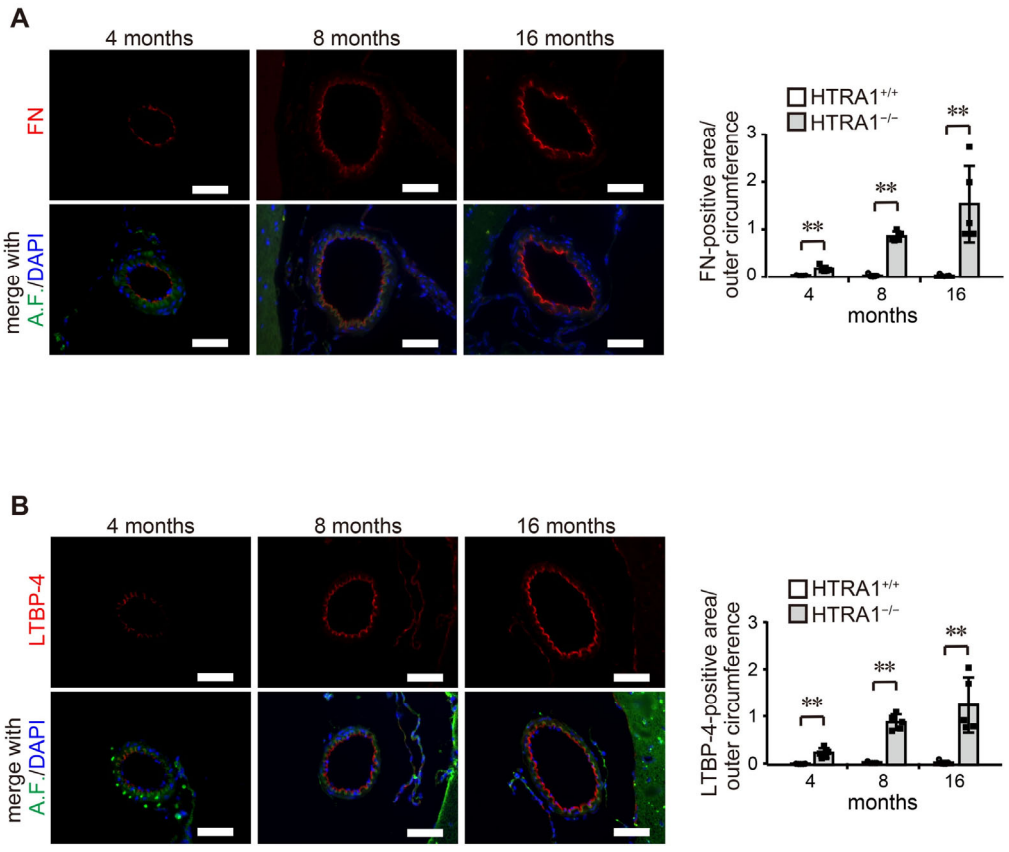

Supplemental Figure 10. Vascular accumulation of matrisome proteins with age in the cerebral arteries of HTRA1$^{-/-}$ mice. (A and B) Immunohistochemical detection of FN **(A)** and LTBP-4 **(B)** in the anterior cerebral arteries of HTRA1$^{-/-}$ mice at different ages. FN and LTBP-4 were immunodetected at 4, 8, and 16 months of age. Autofluorescence (A.F.) (green). FN and LTBP-4 accumulation in HTRA1$^{-/-}$ mice was obvious at 4 months of age. Scale bar = 50 μm. The bar graphs show quantification of FN- and LTBP-4-immunopositive areas in cross-sections of arteries. The FN- and LTBP-4-immunostained areas in the vessel wall in each image were quantified and normalized to the outer circumference. **$P < 0.01$ with Mann-Whitney U-test (n = 5 animals per group; 3–4 images per animal). The data represent the mean ± s.d.

Supplemental Figure 11

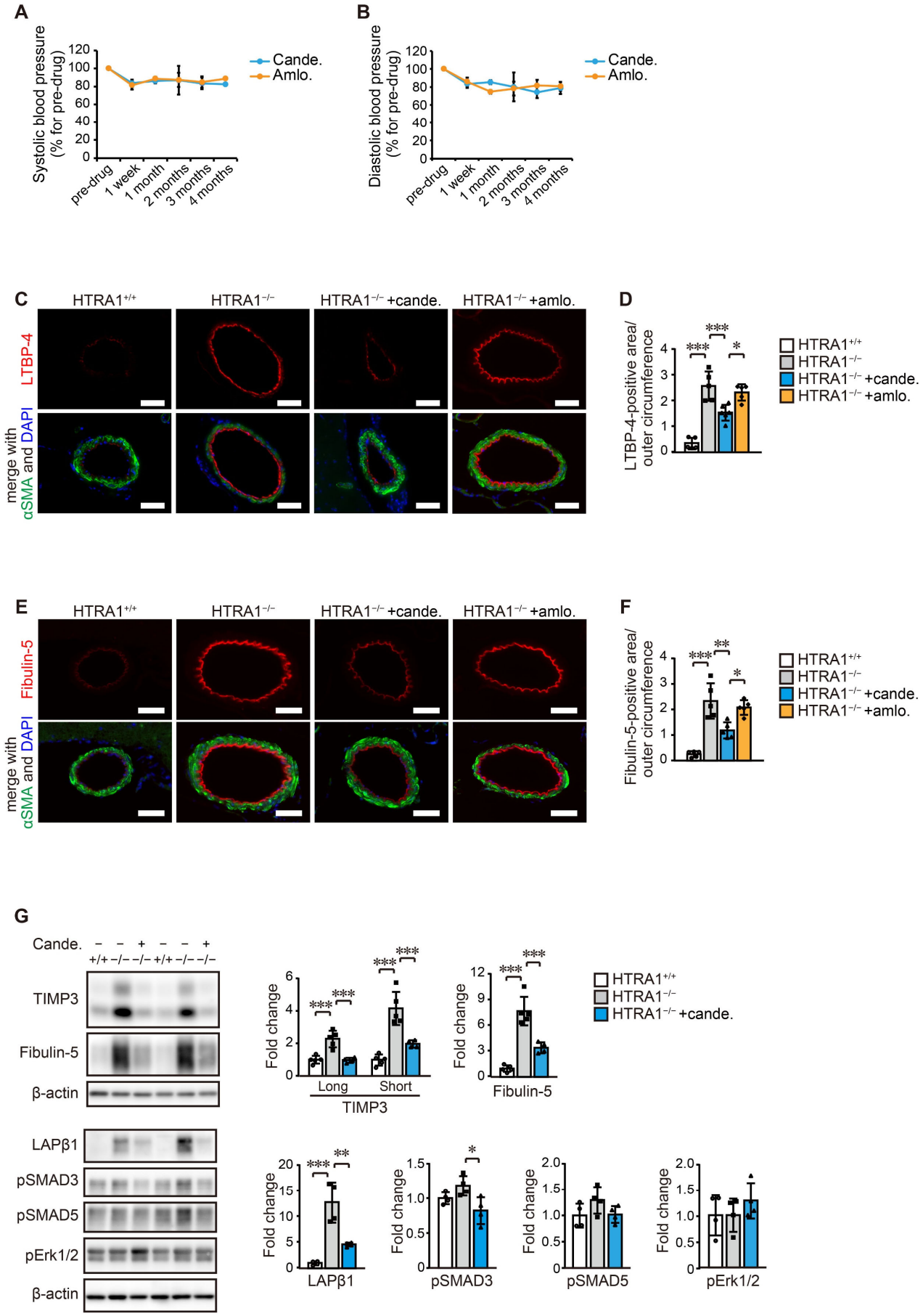

Supplemental Figure 11. Effect of drug treatment on matrisome protein accumulation and signals. (A and B) Percent change in blood pressure following drug administration. Systolic **(A)** and diastolic **(B)** blood pressure of HTRA1$^{-/-}$ mice treated with candesartan or amlodipine (n = 4 animals per group). **(C–F)** LTBP-4 **(C)** and fibulin-5 **(E)** were detected in the anterior cerebral arteries by immunohistochemical staining with medial visualization by αSMA immunostaining at 24 months of age. Scale bar = 50 μm. The area positive for LTBP-4 **(D)** or fibulin-5 **(F)** was quantified and normalized to the outer circumference (n = 5–6 animals per group). **(G)** Quantification of matrisome proteins and level of each signal in the anterior and middle cerebral arteries of 24-month-old HTRA1$^{+/+}$ and HTRA1$^{-/-}$ mice with or without candesartan treatment by immunoblotting analysis (n = 4–5 animals per group). Immunoreactivity was measured by densitometric analysis and normalized to the level of β-actin. The samples used for LAPβ1, pSMAD3, pSMAD5, and pErk1/2 levels in the DOC fraction were the identical to those used in **Figure 4C**, and the same β-actin levels were utilized for normalization. The data represent the mean ± s.d. *P < 0.05, **P < 0.01 and ***P < 0.001 with Bonferroni post hoc test **(D, F and G)**.

Supplemental Figure 12

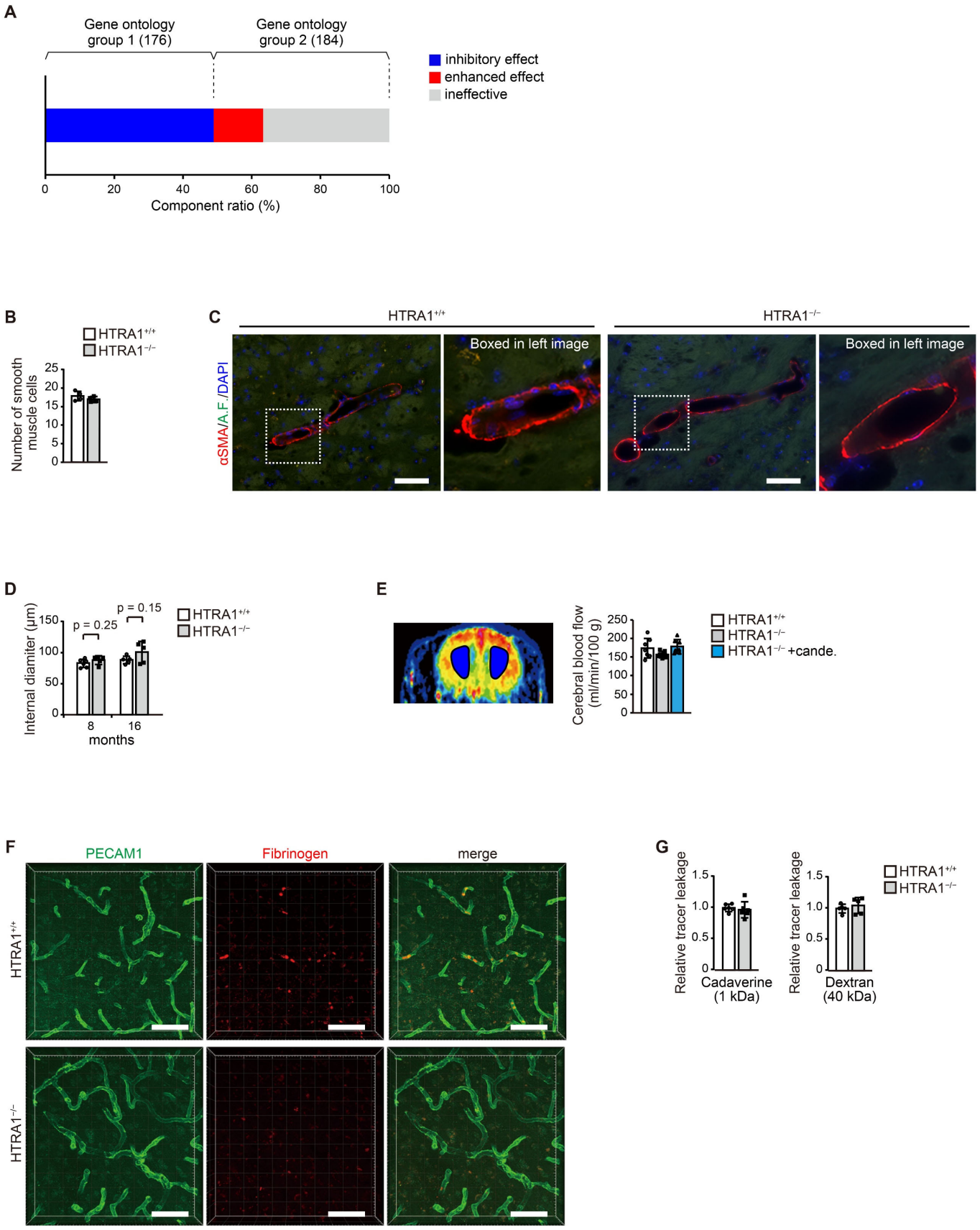

Supplemental Figure 12. Protein classification for GO enrichment analysis, vascular morphological analysis by age, cerebral blood flow in the striatum, and blood-brain barrier function. (A) Details of the groups for GO enrichment analysis shown in Figure 4D. In the 2nd MS analysis, proteins on which candesartan showed an inhibitory effect against increasing changes in HTRA1$^{-/-}$ mice compared to HTRA1$^{+/+}$ mice were classified as group 1, and proteins on which candesartan enhanced the increasing changes in HTRA1$^{-/-}$ mice (enhanced effect) or had no effect (ineffective) were classified as group 2. The bar graphs show the percentages for each category. The numbers in parentheses indicate the actual number of proteins classified from the 2nd MS analysis. **(B)** The number of vascular SMCs on the anterior cerebral arteries was quantified by counting the nuclei of αSMA-positive cells at 24 months of age (n = 4 animals per group, 10–14 images per animal). **(C)** Immunohistochemical observation of SMCs in parenchymal arterioles. Scale bar = 50 μm. **(D)** The vascular internal diameter was measured from αSMA and PECAM1 immunostained cross-sectional vasculature images of samples from mice aged 8 and 16 months (n = 5–6 animals per group). Two-tailed unpaired t-test. **(E)** The resting cerebral blood flow in the striatum was calculated from the regions of interest in the bilateral hemisphere, which are the blue regions in the image (n = 7 animals per group). **(F and G)** Blood-brain barrier permeability was examined in 24-month-old HTRA1$^{+/+}$ and HTRA1$^{-/-}$ mice. **(F)** Plasma extravasation was examined by immunostaining for fibrinogen at 24 months of age. Brain slices from which intravascular blood was removed by transcardial perfusion were subjected to immunostaining for fibrinogen. Although fibrinogen deposition in the vessel lumen was occasionally observed, there was no appreciable extravasation into the brain parenchyma (n = 3 animals per genotype). Scale bar = 50 μm. **(G)** Extravasation of intravenously injected fluorescence tracer into the cerebrum was quantified after 2 h of circulation. Cadaverine (1 kDa) and TMR-dextran (40 kDa) were used as tracers (n = 5–6 animals per group). The data represent the mean ± s.d.

Supplemental Figure 13

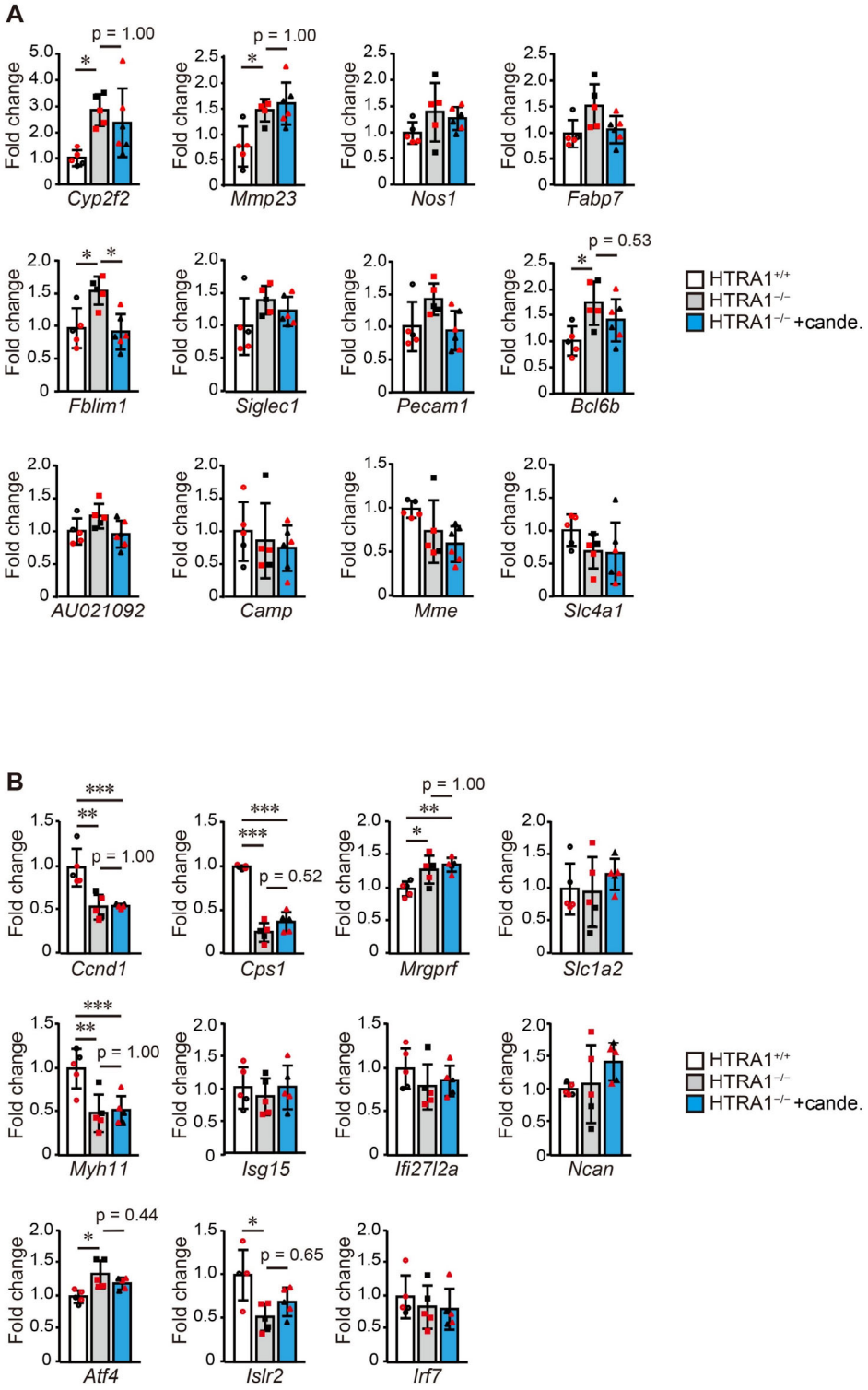

Supplemental Figure 13. Verification of differentially expressed genes identified by RNA-seq analysis. **(A and B)** We conducted ddPCR analysis to verify the differentially expressed genes between HTRA1$^{+/+}$ and HTRA1$^{-/-}$ mice and between untreated HTRA1$^{-/-}$ mice and HTRA1$^{-/-}$ mice subjected to short-term **(A)** or long-term **(B)** candesartan treatment with more samples. Data from 4-month-old **(A)** and 24-month-old **(B)** mice are shown (n = 5–6 animals per group). The bar graphs show the value relative to that of HTRA1$^{+/+}$ mice. The red dots indicate samples used in the RNA-seq analysis. RNA extraction and cDNA synthesis were performed simultaneously for all samples. The data represent the mean ± s.d. *P < 0.05, **P < 0.01, and ***P < 0.001 with Bonferroni post hoc test.

Supplemental Figure 14

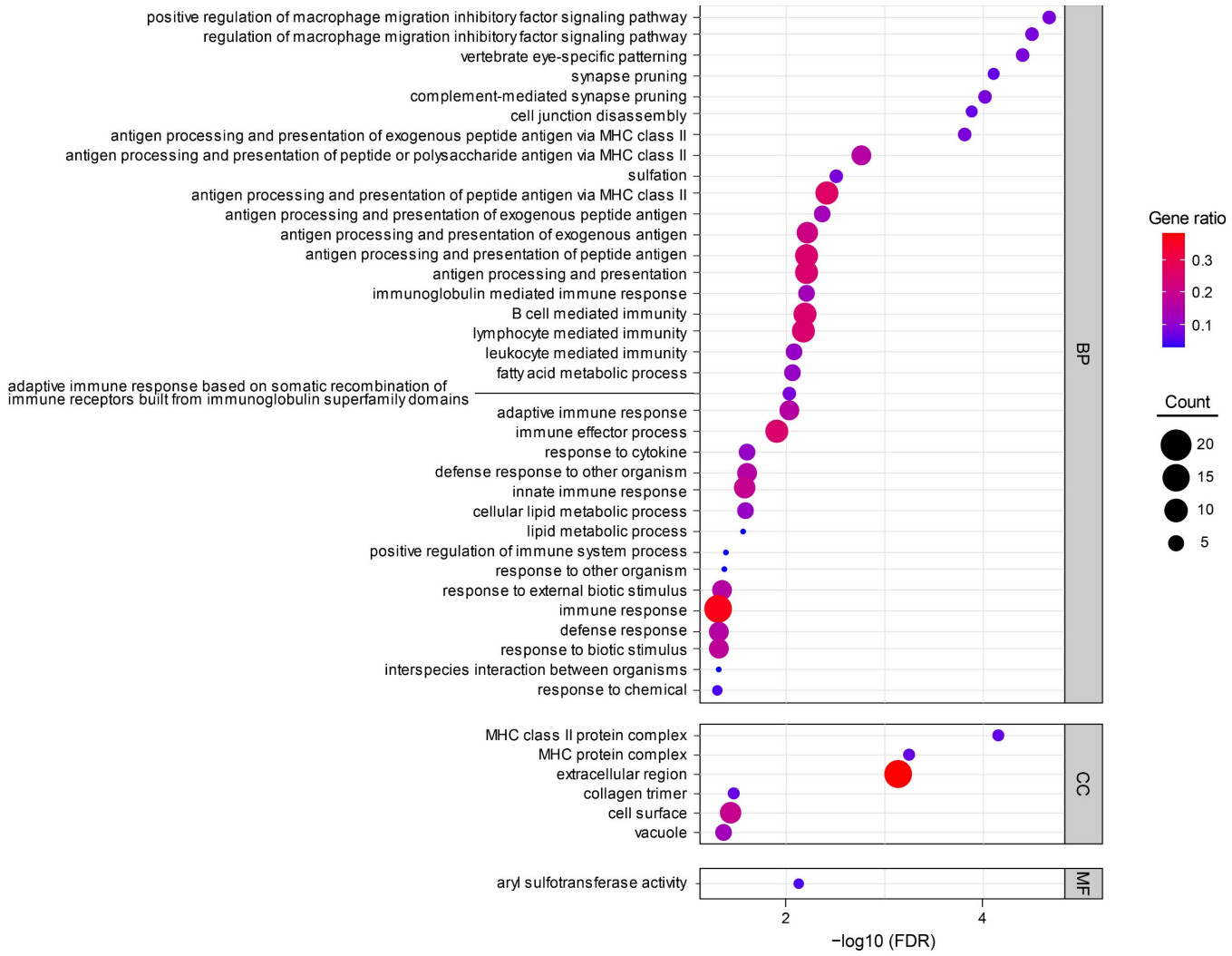

Supplemental Figure 14. GO enrichment analysis of genes downregulated by long-term candesartan treatment. GO enrichment analysis of downregulated genes in cerebral arteries of HTRA1$^{-/-}$ mice subjected to long-term candesartan treatment. The plots are size-scaled by the number of changed proteins enriched for each GO term and color-scaled by gene ratio. BP: biological process, CC: cellular component, MF: molecular function. No significant GO enrichment terms were found for genes upregulated by long-term candesartan treatment, differentially expressed genes between HTRA1$^{+/+}$ and HTRA1$^{-/-}$ mice or differentially expressed genes between untreated HTRA1$^{-/-}$ mice and HTRA1$^{-/-}$ mice subjected to short-term candesartan treatment.

Supplemental Figure 15

A

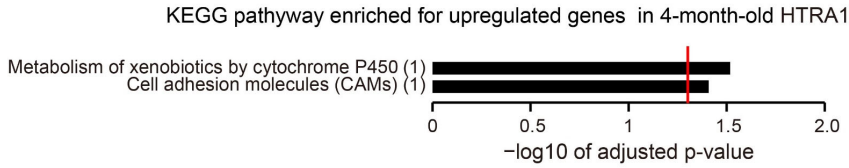

B

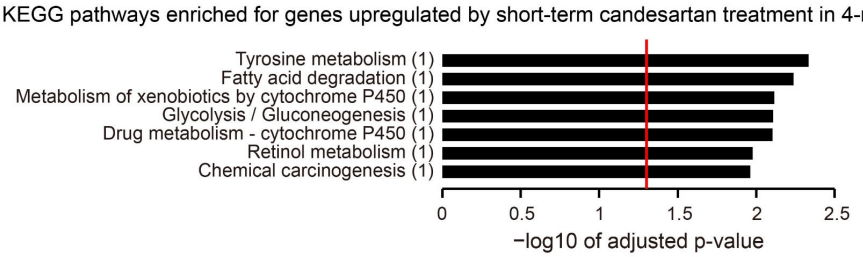

C

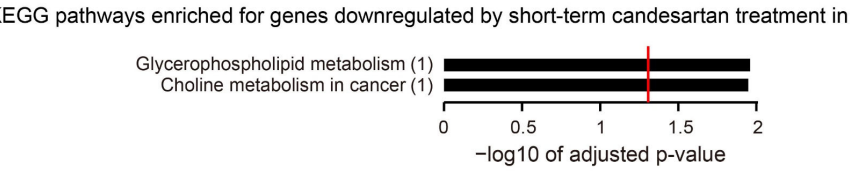

D

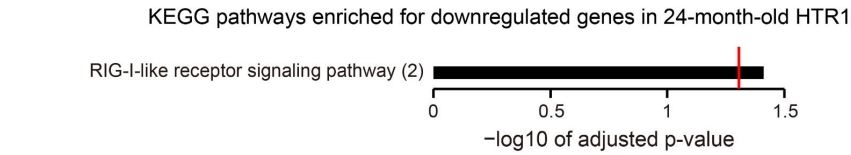

E

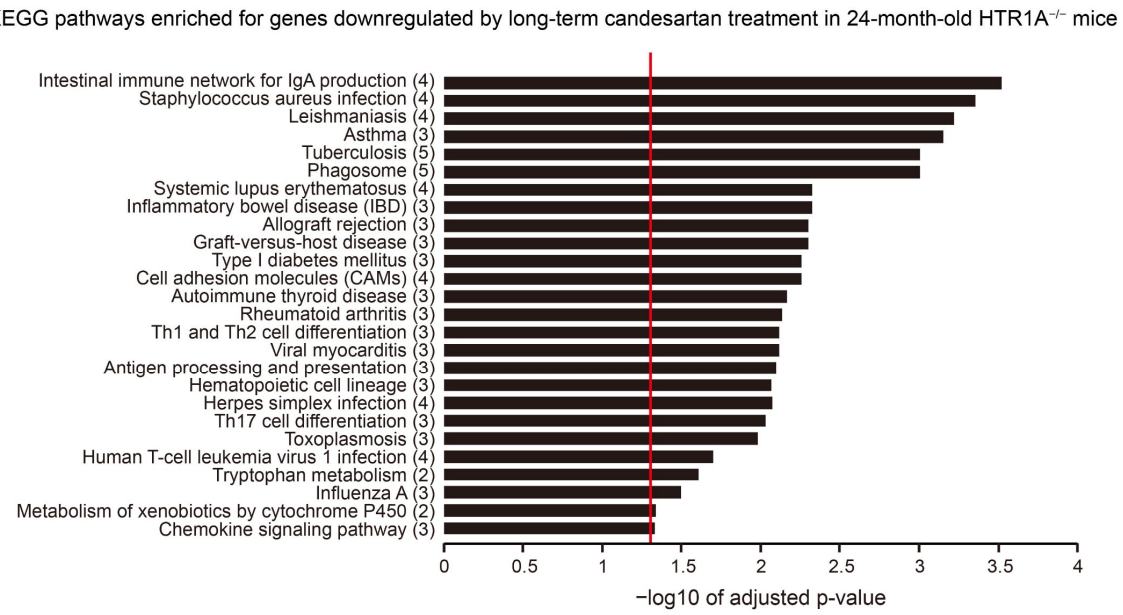

Supplemental Figure 15. KEGG pathway analysis of RNA-seq data from 4-month-old and 24-month-old mice. (A–C) KEGG pathway analysis of data from 4-month-old mice. **(A)** Pathway enrichment charts displaying pathways enriched for genes that were upregulated in the cerebral arteries of $HTRA1^{-/-}$ mice compared with those of $HTRA1^{+/+}$ mice at 4 months of age. **(B and C)** Pathway enrichment charts displaying pathways enriched for genes that were upregulated **(B)** or downregulated **(C)** in candesartan-treated 4-month-old $HTRA1^{-/-}$ mice compared with untreated mice. **(D and E)** KEGG pathway analysis of data from 24-month-old mice. **(D)** Pathway enrichment charts displaying pathways enriched for genes that were downregulated in the cerebral arteries of $HTRA1^{-/-}$ mice compared with those of $HTRA1^{+/+}$ mice at 24 months of age. **(E)** Pathway enrichment charts displaying pathways enriched for genes that were downregulated in 24-month-old $HTRA1^{-/-}$ mice treated with candesartan from 4 to 24 months of age compared with untreated $HTRA1^{-/-}$ mice. The red lines indicate results that were significant with an adjusted p-value < 0.05. Enrichment is shown as $-\log10$ of the adjusted p-value ($n = 3$ animals per group). No significant enrichment was found among the other groups.

Supplemental Table 17. List of PCR primers.

Genotyping

Construct name	Forward primer sequence (5′ to 3′)	Reverse primer sequence (5′ to 3′)
Wild-type locus	AGGGTCTCAAGTATCCAGGTTGTCC	GTTAAAGTTGGGCCTGGCTCTTCC
Mutant locus	AGGGTCTCAAGTATCCAGGTTGTCC	ATAAACCCTCTTGCAGTTGCATC

RT-PCR

Construct name	Forward primer sequence (5′ to 3′)	Reverse primer sequence (5′ to 3′)
Htra1	AAATTCCGGAGGCCCGTTA	TCGATCGTGGGACTCTGTC

Supplemental Table 18. Clinical data of patients used for immunohistochemical analysis.

		Disease	Age (years)	Sex
CARASIL	CARASIL1	CARASIL (p.Arg343Ter)	46	F
	CARASIL2	CARASIL (p.Arg343Ter)	54	M
Controls	C1	Extensive peripheral neuropathy	49	F
	C2	Aortic dissection	89	M
	C3	Panperitonitis	51	M
	C4	Guillain-Barré syndrome	51	F

M: male; F: female

Supplemental methods

Measurements of blood pressure and blood glucose levels

Blood pressure was measured in conscious mice during the daytime via the tail-cuff method (Softron, Tokyo). Mouse blood glucose levels were measured with the Arkray Glucocard Diameter-alpha system (GT-1661, Arkray, Inc.).

qRT-PCR

qRT-PCR was performed with SYBR Green Premix ExTaq II (Takara Bio Inc.). The expression levels of the target gene relative to those of two housekeeping genes were determined using the ΔΔCT method.

Electron microscopy

The mice were transcardially perfused with HBSS followed by a fixative solution containing 4% paraformaldehyde and 0.1% glutaraldehyde. Isolated brains were immersed in the same fixative solution overnight at 4°C and rinsed with PBS at 4°C until use. The brains were sliced into 2-mm-thick sections. Slices containing the hippocampus and the striatum were sectioned into 2-mm^3 blocks that included pial arteries (the anterior cerebral artery). The brain blocks were dehydrated with an increasing concentrations of N,N-dimethyl formamide (DMFA) from 50% to 100% at −25°C. Subsequently, the brain blocks were incubated with a 1:1 solution of DMFA:LR-White for 15 minutes at −25°C and with a 1:2 solution of DMFA:LR-White for 15 minutes at −25°C. Finally, the blocks were embedded in LR-White for 24 hours using a UV irradiator at −25°C. Ultrathin sections were cut from the blocks using an ultramicrotome (Leica) and collected on separate foramen grids. The sections were stained with uranyl acetate for 10 minutes and lead citrate solution for 7 minutes.

Immunohistochemistry was performed using 4 μm sections from paraffin-embedded blocks of tissue from HTRA1$^{-/-}$ mice. The sections were pretreated with enzyme digestion (proteinase K) for 10 seconds. The sections were permeabilized in 1% BSA and 0.1% Triton X-100 at room temperature for 1 hour and incubated with a rabbit anti-FN antibody (ab2413; 1:250; Abcam) overnight at 4°C. Labeling was visualized with a biotinylated anti-rabbit IgG antibody (1:200; Vector Lab) and avidin-biotin-horseradish peroxidase (Vectastain ABC kit; Vector Lab) with 3,3′-diaminobenzidine tetrahydrochloride (Vector Lab). An adjacent paraffin-embedded section stained with eosin was used as a color reference. Both sections were subjected to dehydration, permeabilized, and then covered by slide glasses with a conventional sealant, and fields containing pial arteries were identified. The slide glasses were scratched to mark the location of the pial arteries, and then the sections were soaked in xylene overnight to remove the cover. The sections were hydrated with decreasing concentrations of ethanol and rinsed in PBS. All parts of each section except for the pial arteries were removed with a scalpel. After incubation with osmium tetraoxide for 10 minutes at room temperature, the sections were dehydrated with increasing concentrations of ethanol and incubated with epon resin diluted with propylene oxide. The sections were embedded in epon resin for 24 hours at 62°C. Ultrathin sections were cut from the blocks using an ultramicrotome and collected on solitary foramen grids. Brightfield transmission electron microscopy images of brain sections were acquired using a HITACHI HT7700 at an acceleration voltage of 75 kV.

HTRA1 digestion assay

Recombinant C-terminus myc-His6-tagged human full-length HTRA1 protein and S328A HTRA1 protein containing a mutation in the protease active site were used. These proteins were expressed in FreeStyle 293 cells (Thermo Fisher Scientific). HTRA1 recombinant protein was purified from cell-conditioned media using a HisTrap FF crude

column (GE Healthcare). One microgram of human LTBP-4 protein (R&D System), human FN (R&D System), or human tropoelastin (Sigma) was incubated with a stepwise concentration of purified recombinant human HTRA1 protein in Tris-HCl (pH 8.0) and 150 mM NaCl at 37°C for 6 h, and then immunoblotting analysis was performed.

Primary culture

Primary cultures of cortical neurons, astrocytes, microglia, and cerebrovascular endothelial cells were prepared as described elsewhere. Briefly, neurons were prepared from the cortices of embryonic day 15 HTRA1$^{+/+}$ mice. The leptomeninges were removed from the cortex. The cortices were dissociated using Nerve-Cell Dissociation Solution CP (DS Pharma Biomedical) according to the manufacturer's instructions. The cells were seeded on poly-D-lysine-coated six-well microplates in neuronal medium (DS Pharma Biomedical). To eliminate proliferative cells, cytarabine (Ara-C) was added to the medium, and the cells were incubated for 48 hours.

For astrocyte culture, the leptomeninges-free cortices of postnatal day 1 mouse brains were dissociated using trypsin and seeded in noncoated flask dishes in DMEM supplemented with 10% fetal bovine serum (FBS) (mixed glial cell culture). Confluent cells were passaged three times to eliminate undesired cells.

Microglia were obtained from preseeded mixed glial cells cultured as described. On days 21 to 28 in vitro, microglia were collected from the cultures by shaking the flasks at 125 rpm for 4 to 5 hours. Floating microglia were collected and seeded in noncoated plastic dishes. After incubation for 1 hour, the attached microglia were purified by washing with PBS to remove the nonadherent cells.

Vascular endothelial cells were prepared from the brains of 4-month-old mice using a puromycin purification method (5). Isolated cortices from which the meninges and white matter were removed were minced with a scalpel and digested with 30 U/ml papain at 37°C for 70 min. The digested tissues were triturated with an 18-G needle and

then a 21-G needle. After the addition of a 1.7-fold volume of 22% FBS, the tissues were centrifuged at 2,000×g for 10 minutes at 4°C. The upper layer of debris was discarded, and precipitated microvessels were suspended in VascuLife microvascular endothelial cell medium (VascuLife® EnGS-Mv Microvascular Endothelial Kit; Lifeline Cell Technology) and seeded in fibronectin- and collagen IV-coated microplates. After 24 hours in vitro, the culture medium was changed to medium comprising 4 μg/ml puromycin to select vascular endothelial cells. After incubation with puromycin for 2 days, the medium was changed every 3 days until confluent.

Quantification of FN levels in plasma

FN levels in plasma were quantified with a mouse fibronectin ELISA kit (Abcam) according to the manufacturer's guidelines.

Intravenous injection of tracers and detection of injected tracers

Tracers were intravenously injected into 24-month-old mice via the tail vein. The following tracers were used: cadaverine conjugated to Alexa Fluor 555 (6 μg/g body weight) (Thermo Fisher Scientific) and 40 kDa tetramethylrhodamine (TMR)-dextran (40 μg/g body weight) (Thermo Fisher Scientific). After 2 h of circulation, to quantify the amount of tracer in the brain, anaesthetized animals were perfused for 5 min with HBSS, and the brains were removed and homogenized in 1% Triton X-100 in PBS (pH 7.2). The brain lysates were centrifuged at 15,000 × g for 30 min, and the relative fluorescence intensity of the supernatant was measured with a fluorometer (excitation/emission, 540/590 nm; FilterMax™ F5 Multi-Mode Microplate Reader; Molecular Devices). The measured fluorescence intensity of each sample was normalized to brain weight.

ddPCR

cDNA was synthesized with a SuperScript VILO™ cDNA Synthesis Kit (Thermo Fisher Scientific). We used the Bio-Rad QX200 ddPCR system (Bio-Rad). Each reaction was performed in a 20-μl system consisting of 10 μL ddPCR™ Supermix for Probes No

dUTP (Bio-Rad), 1 μM primers, 250 nM probe, and template cDNA. Droplets containing the PCR mixture were formed using the Bio-Rad QX-100 emulsification device. After PCR cycling, the droplets were analyzed immediately by QuantaSoft v.1.6 (Bio-Rad). Suitable housekeeping genes were analyzed using a mouse housekeeping gene primer set (Takara Bio Inc.) and geNorm software. The expression level of each gene was normalized to the expression level of the reference gene set. Predesigned primers and probes (5'/FAM/ZEN/IBFQ/3') were purchased from Integrated DNA Technologies. The primer and probe sequences are available on request.

Fixed mouse brain tissue preparation

Blood was removed by transcardial perfusion with Ca^{2+}-free HBSS at 37 °C and 75 mmHg for 10 min. The perfusion pressure was monitored with a manometer. Brain samples were fixed with 4% paraformaldehyde. For cryosection preparation, the brains were immersed in 30% sucrose in 0.1 M PBS, embedded in optimal cutting temperature (OCT) compound (Sakura Finetek), and sectioned at a thickness of 14 μm with a cryostat (CM1950; Leica). To prepare paraffin sections, the brains were processed for paraffin embedding after dehydration and sectioned coronally at a thickness of 4 μm. For brain capillary analysis, fixed brains were embedded in agarose and cut using a vibratome (Leica) at a thickness of 50 μm. Isoflurane was used for anesthesia for vascular morphometric analysis. For other experiments, halothane was also used.

Immunohistochemistry

For analysis of the human brain, we used formalin-fixed, paraffin-embedded brain specimens obtained from two CARASIL patients and four controls (Supplemental Table 18). For mouse brain tissue analysis, antigen retrieval was performed by boiling in sodium citrate buffer (pH 6.0) in a microwave oven for αSMA, CD31 (PECAM1), TIMP3 and FN staining or by proteinase K-treatment for LTBP-4, LAPβ1, and elastin staining. For

immunostaining of the human brain, both boiling and proteinase K treatment were used for antigen retrieval. Then, the sections were incubated with a biotinylated mouse anti-αSMA antibody (LS-C87562; 1:100; LifeSpan BioScience), rat anti-CD31 (PECAM1) antibody (DIA-310; 1:20; Optistain), rabbit anti-TIMP3 antibody (ab39184; 1:800; Abcam), rabbit anti-FN antibodies (mouse tissue: ab2413; 1:250; Abcam; human tissue: ab32419; 1:200; Abcam), rabbit or goat anti-LTBP-4 antibodies (mouse tissue: sc-33144; 1:20; Santa Cruz Biotech or AF2885; 1:50; R&D Systems; human tissue: CABT-B8442; 1:500; Creative Diagnostics), rabbit anti-elastin antibody (PR-387; 1:500; Elastin Products or sc-58756; 1:100; Santa Cruz Biotech), rabbit anti-fibulin-5 (ab109428; 1:100; Abcam), or goat anti-LAPβ1 antibody (AF-246-NA; 1:50; R&D Systems) overnight at 4 °C. Then, the sections were incubated with Alexa Fluor-labeled secondary antibodies or biotinylated secondary antibodies and visualized using avidin-biotin-horseradish peroxidase with 3,3′-diaminobenzidine tetrahydrochloride. Human brain sections were counterstained with hematoxylin. For simultaneous detection of FN and LTBP-4 or fibulin-5, primary antibodies were labeled fluorescently using Zenon Antibody Labeling Kits (Thermo Fisher Scientific). For endothelial cell visualization, DyLight-594-labeled tomato lectin was also used. Fluorescence microscopy images were obtained using an all-in-one microscope (BioRevo BZ-9000; Keyence) or a confocal laser microscope (LSM710; Carl Zeiss).

Vibratome sections were blocked and incubated with a rat anti-CD13 antibody (R3-63; 1:50; AbD Serotec), rat CD31 (PECAM1) antibody (DIA-310; 1:20; Optistain), or rabbit anti-fibrinogen antibody (A0080; 1:250; Dako). Three-dimensional images were obtained using confocal laser microscopy. The vascular length was measured using the Filament Tracer function of Imaris software (version 6.2.0; Bitplane).

In situ hybridization

A digoxigenin-labeled RNA probe corresponding to nucleotides 1248–1803 of mouse *Htra1* was synthesized by in vitro transcription. The probe templating cDNA fragments was amplified by PCR. Frozen coronal sections were pretreated with proteinase K, acetylated, and hybridized with riboprobes (1 μg/mL). After hybridization, the sections were thoroughly washed at 60 °C, treated with RNase, and finally washed at 37 °C. To detect the hybridized probe, the sections were incubated with an alkaline phosphatase (AP)-conjugated sheep anti-digoxigenin antibody (Roche). AP activity was visualized with NBT/BCIP solution (Roche). For immunohistochemistry combined with in situ hybridization, frozen brain sections were incubated with the corresponding primary antibodies after RNase A treatment. The primary antibodies used for this analysis were rabbit anti-GFAP antibody (G9269; 1:200; Sigma), biotinylated mouse anti-αSMA antibody (LS-C87562; 1:50; LifeSpan BioScience Inc.), rat anti-CD13 antibody (R3-63; 1:10; AbD Serotec), anti-Iba-1 antibody (019-19741; 1:200; Wako), and rabbit anti-NeuN antibody (ABN78; 1:200; EMD Millipore). Then, the sections were incubated with the AP-conjugated anti-digoxigenin antibody and fluorophore-labeled secondary antibodies or Alexa Fluor 488-labeled streptavidin. To visualize the immunoreactivity of the anti-digoxigenin antibody, we used an HNPP Fluorescent Detection Kit (Roche).

Vascular morphometric analysis

Vascular histology was conducted according to previous studies (6, 7). For morphometric analysis of pial arteries, we selected and analyzed micrographic images of cross-sections of pial arteries (anterior cerebral artery: lumen diameter, 80–100 μm in $HTRA1^{+/+}$ mice) in coronal brain slices (bregma: +0.86 to −2.30 mm) at equal intervals and avoided arterial branching points using 5 to 7 images per animal for each analysis. Cerebrovascular endothelial cells and vascular SMCs were visualized by immunostaining using antibodies against CD31 (PECAM1) and αSMA (see the Immunohistochemistry section). The lumen circumference was measured from CD31 staining images using

macros in ImageJ (https://www.ipmc.cnrs.fr/~duprat/scripts/). Similarly, the medial internal and external circumferences were measured according to the internal and external boundaries of the αSMA-positive area. The vascular lumen diameter was calculated from the luminal internal circumference. The medial CSA was measured using the αSMA-positive area. Intimal thickness was measured using the medial internal boundary of the αSMA-positive area and the CD31 layer. The intimal thickness in each image was determined by measuring and averaging 20 to 30 points per image. CSA and intimal thickness were analyzed using Imaris software (version 6.2.0, Bitplane). The number of αSMA-positive cell nuclei was counted with Imaris software.

References

1. Grant RI, et al. Organizational hierarchy and structural diversity of microvascular pericytes in adult mouse cortex. *J Cereb Blood Flow Metab.* 2019;39(3):411–425.
2. Naba A, et al. The matrisome: in silico definition and in vivo characterization by proteomics of normal and tumor extracellular matrices. *Mol Cell Proteomics.* 2012;11(4):M111.014647.
3. Naba A, et al. Towards definition of an ECM parts list: an advance on GO categories. *Matrix Biol.* 2012;31(7-8):371–372.
4. Zellner A, et al. CADASIL brain vessels show a HTRA1 loss-of-function profile. *Acta Neuropathol.* 2018;136(1):111–125.
5. Perriere N, et al. Puromycin-based purification of rat brain capillary endothelial cell cultures. Effect on the expression of blood-brain barrier-specific properties. *J Neurochem.* 2005;93(2):279–289.
6. Castro MM, et al. Metalloproteinase inhibition ameliorates hypertension and prevents vascular dysfunction and remodeling in renovascular hypertensive rats. *Atherosclerosis.* 2008;198(2):320–331.
7. Retailleau K, et al. Piezo1 in Smooth Muscle Cells Is Involved in Hypertension-Dependent Arterial Remodeling. *Cell Rep.* 2015;13(6):1161–1171.

Full unedited images for Figure 2A

Fibronectin

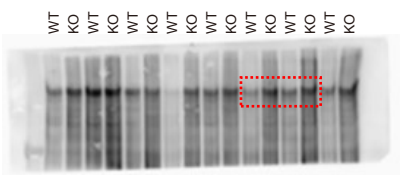

LTBP-4

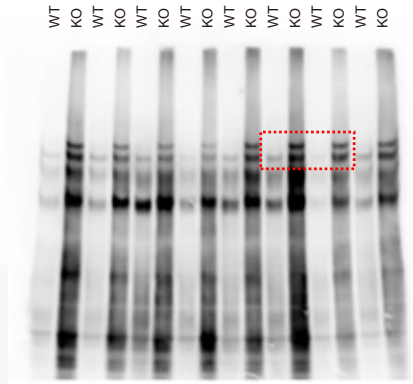

Elastin

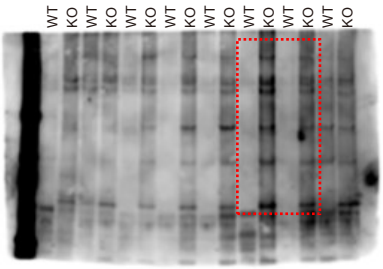

β-actin

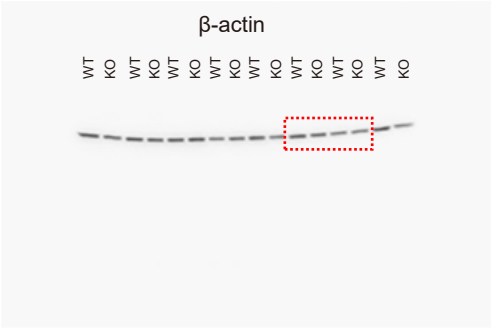

TIMP3

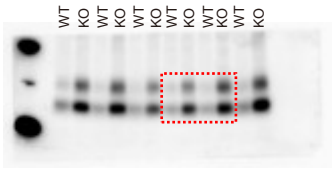

Fibulin-5

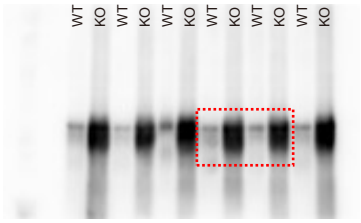

β-actin for TIMP3 and fibulin-5

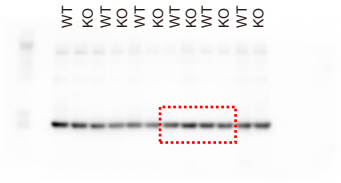

EDA

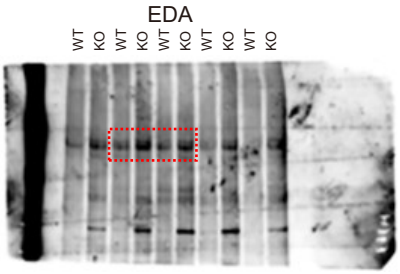

β-actin for EDA

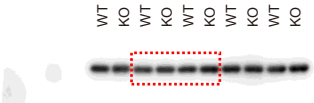

Full unedited images for Figure 4C

Fibronectin

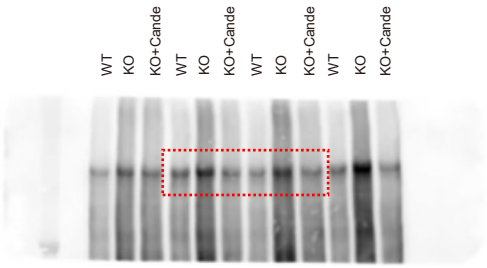

Elastin

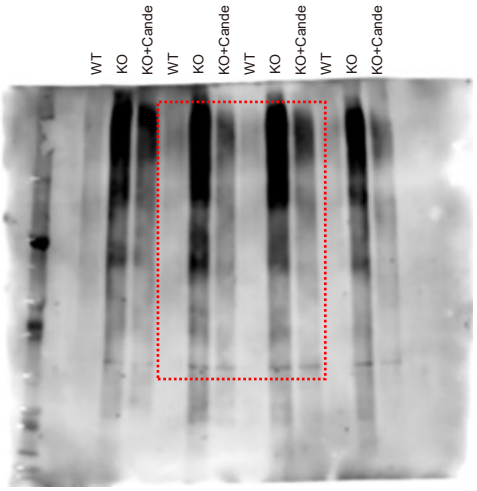

LTBP-4

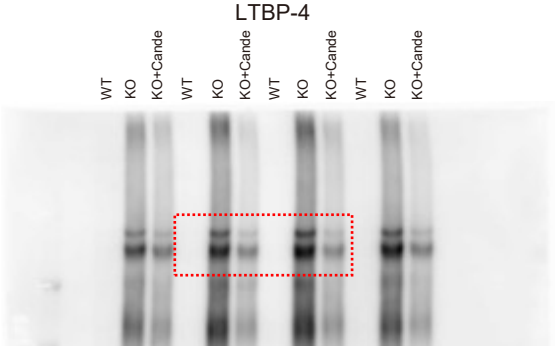

β-actin

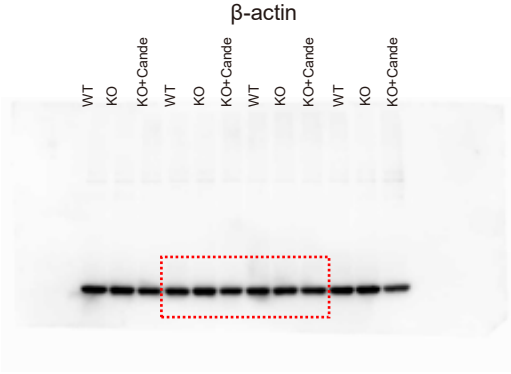

EDA

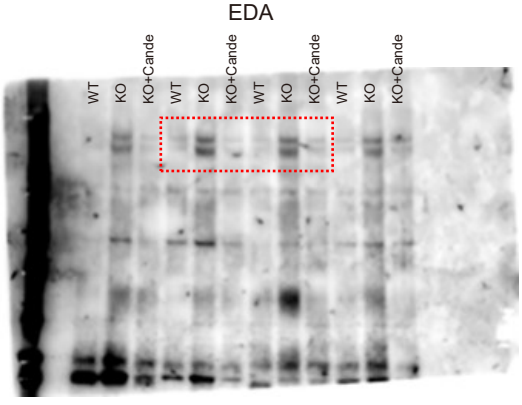

Full unedited images for Supplemental Figure 1B and 1C

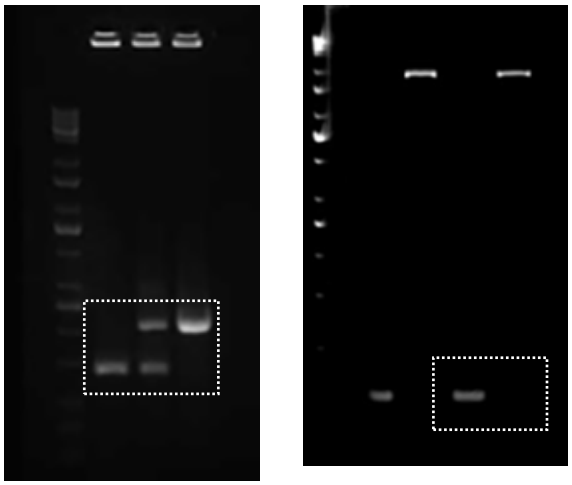

Full unedited images for Supplemental Figure 5A

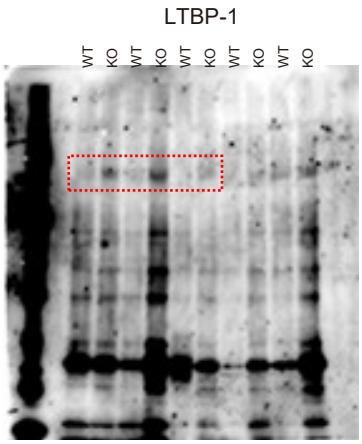

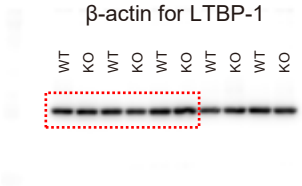

Full unedited images for Supplemental Figure 8A

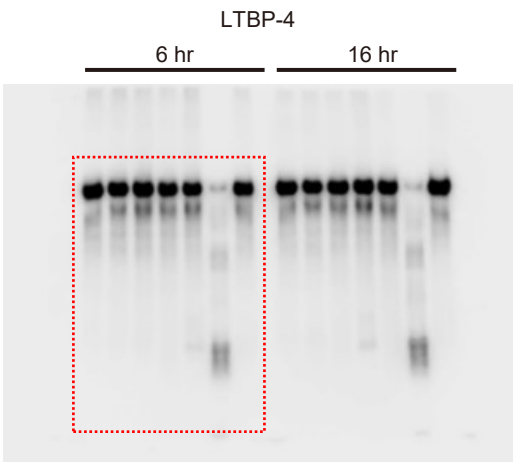

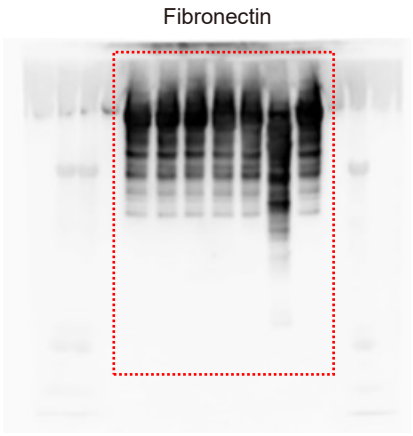

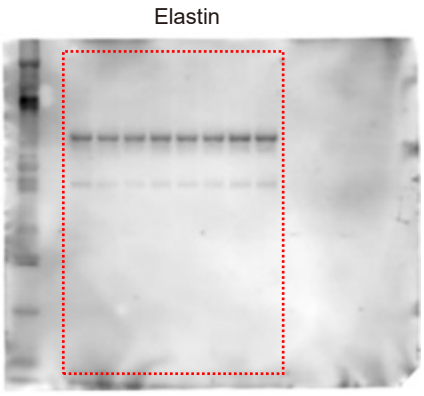

Full unedited images for Supplemental Figure 8B

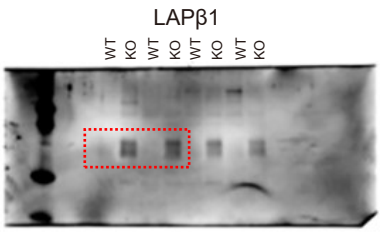

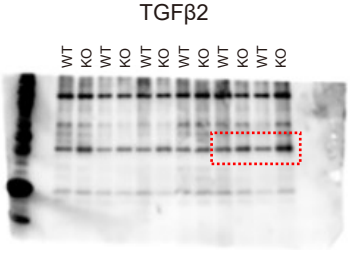

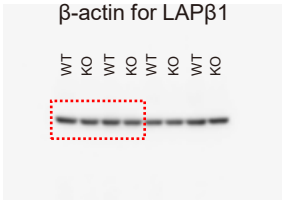

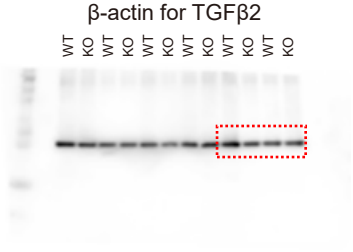

Full unedited images for Supplemental Figure 8F

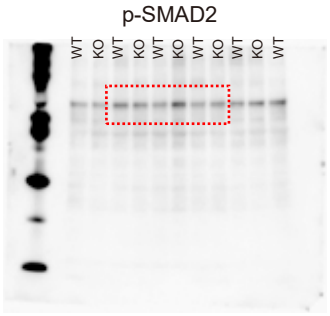

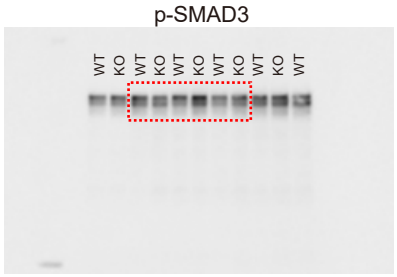

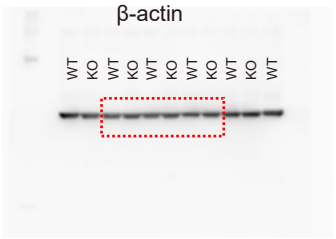

Full unedited images for Supplemental Figure 8G

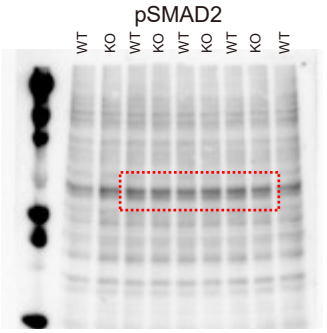

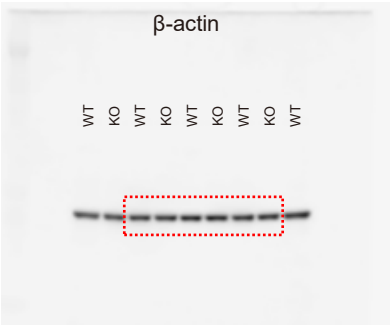

Full unedited images for Supplemental Figure 8J

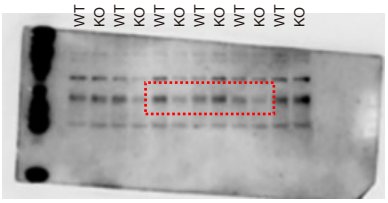

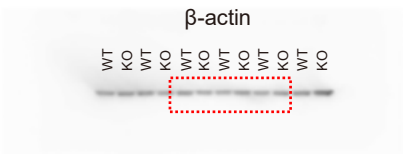

Full unedited images for Supplemental Figure 9A

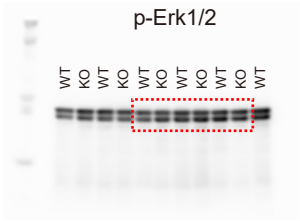

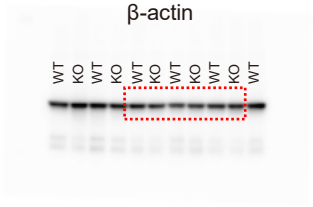

Full unedited images for Supplemental Figure 9B

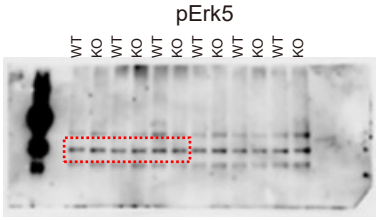

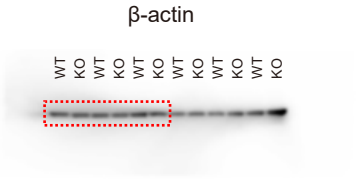

Full unedited images for Supplemental Figure 9C

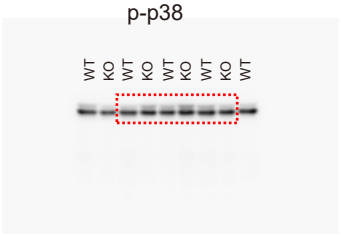

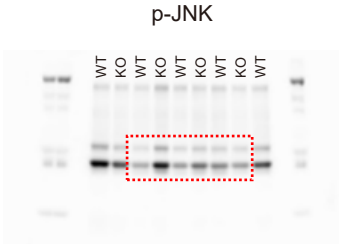

Full unedited images for Supplemental Figure 11G

TIMP3

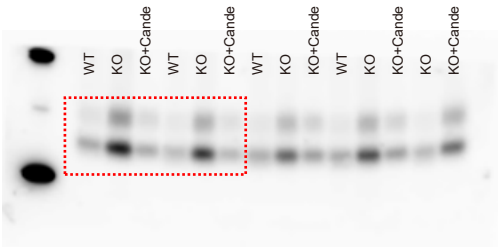

Fibulin-5

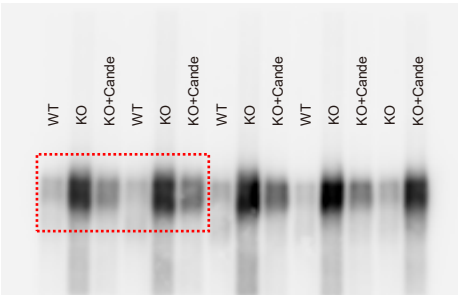

β-actin for TIMP3 and fibulin-5

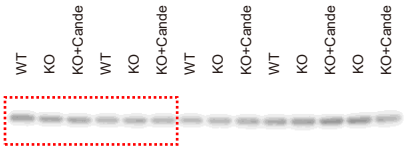

LAPβ1

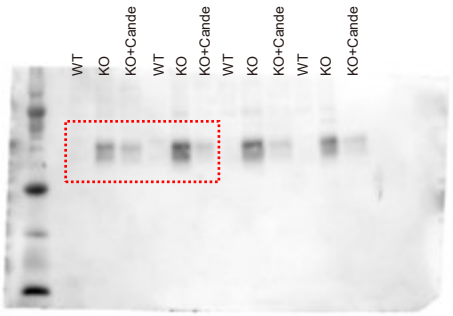

pSMAD3

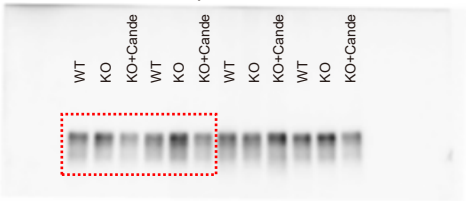

pSMAD5

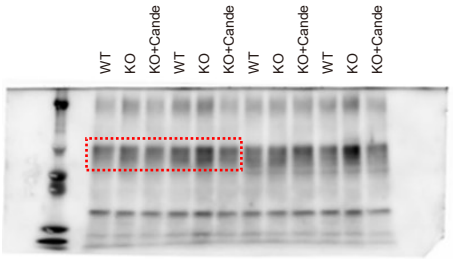

pErk1/2